Pergamon

Prog. Biophys. molec. Biol., Vol. 64, No. 2/3, pp. 237–278, 1995

0079–6107/95 $29.00 + 0.00

PII: S0079–6107(96)00009–0

A FRAMEWORK FOR THE ANALYSIS OF MIXED TIME SERIES/ POINT PROCESS DATA—THEORY AND APPLICATION TO THE STUDY OF PHYSIOLOGICAL TREMOR, SINGLE MOTOR UNIT DISCHARGES AND ELECTROMYOGRAMS

D. M. HALLIDAY,*† J. R. ROSENBERG,* A. M. AMJAD,* P. BREEZE,‡ B. A. CONWAY§ and S. F. FARMER¶

**Division of Neuroscience and Biomedical Systems, Institute of Biomedical and Life Sciences, University of Glasgow, Glasgow, U.K.*
‡Department of Statistics, University of Glasgow, Glasgow, U.K.
§Bioengineering Unit, University of Strathclyde, Glasgow, U.K.
¶The National Hospital for Neurology and Neurosurgery, Queen Square, London, U.K.

CONTENTS

†Author for correspondence at: West Medical Building, University of Glasgow, Glasgow G12 8QQ, U.K.

I. INTRODUCTION

The study of biological systems often results in simultaneous observation of several processes. These may be either a continuously varying waveform, or a sequence of discrete events. In the former case this leads to analyses based on continuous time series, whereas in the latter case the principal quantities available for analysis are the times of occurrence of discrete events, leading to analyses based on stochastic point processes. Examples of such time series include recordings of physiological tremor, surface electromyogram (EMG), electroencephalogram (EEG) signals, and muscle forces or movements. Examples of point processes include the times of occurrence of extracellularly recorded action potentials, such as times of firing of motor unit action potentials and heart action potentials.

A previous report (Rosenberg *et al.*, 1989) presented a set of frequency domain measures for characterizing linear interactions between point process data. The object of the present review is to draw on that material, and extend it to provide a framework for characterizing linear and non-linear interactions between point processes, time series, and hybrids of the two, using estimates of time and frequency domain parameters. The approach adopted is that of spectral estimation procedures based on the finite Fourier transform. Brillinger (1993) points out that spectra have both a theoretical and physical existence, and that it is rare for a concept to have these distinct existences. In practice this means that spectrum analysis can be approached from two very different viewpoints. The statistician is concerned with spectra as theoretical parameters, whereas the experimentalist attempts to gain insight and inference from their data. A combined approach drawing on the expertise of both disciplines is necessary to improve understanding of biological systems, this approach will often involve a multi-disciplinary collaboration between groups of scientists. When analysing experimental data the use of statistics is essential to deal with error and uncertainty, and in the setting up of procedures for testing hypotheses.

Second order (linear) frequency domain parameters are discussed in detail, with examples, in Rosenberg *et al.* (1989) for point process data, and in Brillinger (1981) for time series data. The extension of spectral methods to hybrid data was proposed in Jenkins (1963), and the theoretical foundations are set out in Brillinger (1972, 1974). In the present review the techniques in Rosenberg *et al.* (1989), and Brillinger (1981) are extended to the case of hybrid point process/time series data. In most cases the extension to hybrid data follows naturally as a result of the theory developed in Brillinger (1972). The large sample distribution of the various parameter estimates is also given, and in the linear case these follow from, and are identical to, previous results for point process data and time series data.

Application of the techniques is illustrated by a detailed analysis of a single data set, consisting of four processes, to answer specific questions posed about the processes, and their interaction. The data set consists of simultaneously recorded finger tremor, surface EMG and two single motor units from a normal healthy subject. The theme developed in this review is that by using a variety of procedures, where any one technique may illustrate only one aspect of the data, it is possible to obtain useful insight into the mechanisms controlling the behaviour of complicated systems such as those responsible for generation of physiological tremor. The analysis uses estimates of both time domain and frequency domain parameters, and stresses the complementary nature of time and frequency domain parameters which can be used to characterize different aspects of the same data. The fact that all linear time domain parameters are estimated via the frequency domain does not, in general, affect the interpretation of these parameters. Rosenberg *et al.* (1989) discuss the complementary aspect of time and frequency domain analysis and point out that although certain time and frequency domain parameters are mathematically equivalent, this does not result in equivalence of representation. Thus it is necessary to use both representations to obtain the maximum insight into and inference about the behaviour of complex systems.

The present framework has the added advantage in the linear case of being applicable to both pure time series data and pure point process data. This follows from the Fourier based estimation procedures, where all linear parameters (including time domain parameters) are estimated via the frequency domain. An important part of the present analysis is the use of confidence limits for all parameter estimates. The experimentalist often fails to distinguish between a parameter and its estimate, once a parameter of interest has been defined, an estimation procedure can be developed, which for a finite amount of data will have some associated error. Confidence limits should form an essential part of any statistical analysis, since they provide a guide to interpretation of estimates and allow the significance of any interesting features in parameter estimates to be assessed.

This review is aimed at experimentalists who have suitable data to analyse. The aim is to present the methodologies in sufficient detail to allow the interested researcher to implement a similar analysis. The statistical presentation is kept to a minimum, with the derivation and proofs of the various relationships omitted, these can be found in the referenced material. The review begins in section II with a description of the experimental data and the specific questions about the data which we will address in the present analysis. In section III, we set down a number of definitions and assumptions about the data, which form the basis for the mathematical framework. All linear parameters are estimated via the frequency domain using Fourier methods, the finite Fourier transforms of time series and point process data are discussed in section IV. The next three sections deal with the definition of and estimation procedures for parameters to characterize linear processes and their pairwise interactions (section V), the setting of confidence limits for these parameters (section VI) and examples of the application and interpretation of these parameters (section VII). Sections VIII to X deal with the extension of these parameters to multivariate linear data, and sections XI to XIII deal with the specific case of the identification of multivariate linear systems. The final group of sections XIV to XVI deals with the extension to higher order analyses. The sections on the application and interpretation of parameter estimates (VII, X, XIII and XVI) can be read independently of the methodological sections.

The previous study by Rosenberg *et al.* (1989) includes a brief historical background on point process data analysis, a history of time series analysis based on Fourier methods may be found in Brillinger (1981), and a historical perspective on spectral estimation can be found in Robinson (1982).

II. EXPERIMENTAL METHODS, DESCRIPTION OF DATA, AND QUESTIONS TO BE ADDRESSED

The data set consists of simultaneous recordings of finger tremor, two motor unit spike trains, and a surface electromyogram (EMG) from a normal healthy subject. The tremor signal was derived from an accelerometer fixed to the distal phalanx of the unsupported middle finger. The subject's other fingers, wrist and forearm were all supported and immobilized by a custom designed rigid polypropylene cast. During data collection the subject was asked to extend and maintain the middle finger in a horizontal position. Two single motor units were recorded from a pair of concentric needle electrodes (Medelec DFC25) inserted into the extensor digitorum communis muscle. The surface EMG signal was obtained from a pair of Ag/AgCl bipolar electrodes placed about 20 mm apart on either side of the needles.

The accelerometer output was amplified to a level of 3 V/1 g acceleration, and fed to a data collection interface for digitizing. The band-width of this signal is determined by the characteristics of the accelerometer (Entran EGAX-5) which has a flat frequency response from DC to about 200 Hz. The surface EMG signal was filtered (3–500 Hz), and amplified ($\times 1000$) before digitizing. The needle electrode signals were amplified and band pass filtered before being passed through window discrimination devices. The TTL pulses output from these were fed to the digital input of the data collection device.

The duration of the data set is 180 sec, with motor unit spike times recorded to the

nearest 1 msec, and acceleration and surface EMG signals sampled at 1 msec intervals. Figure 1 shows a 5-sec segment from each of the four processes, in Fig. 1a, b the motor unit spike trains are shown as instantaneous frequency plots, Fig. 1c shows the acceleration record and Fig. 1d the EMG record. Interval histograms for the two motor unit discharges are shown in Fig. 2a, b, respectively, plotted up to 250 msec. The first motor unit spike train, motor unit 0, has 2202 spikes, giving a mean rate of 12.2 spikes/sec, with a coefficient of variation (c.o.v.) of 0.17. The corresponding figures for the second motor unit, motor unit 1, are 1855 spikes, 10.3 spikes/sec and c.o.v. of 0.29. Amplitude histograms are shown in Fig. 2c, d for the complete acceleration and EMG records,

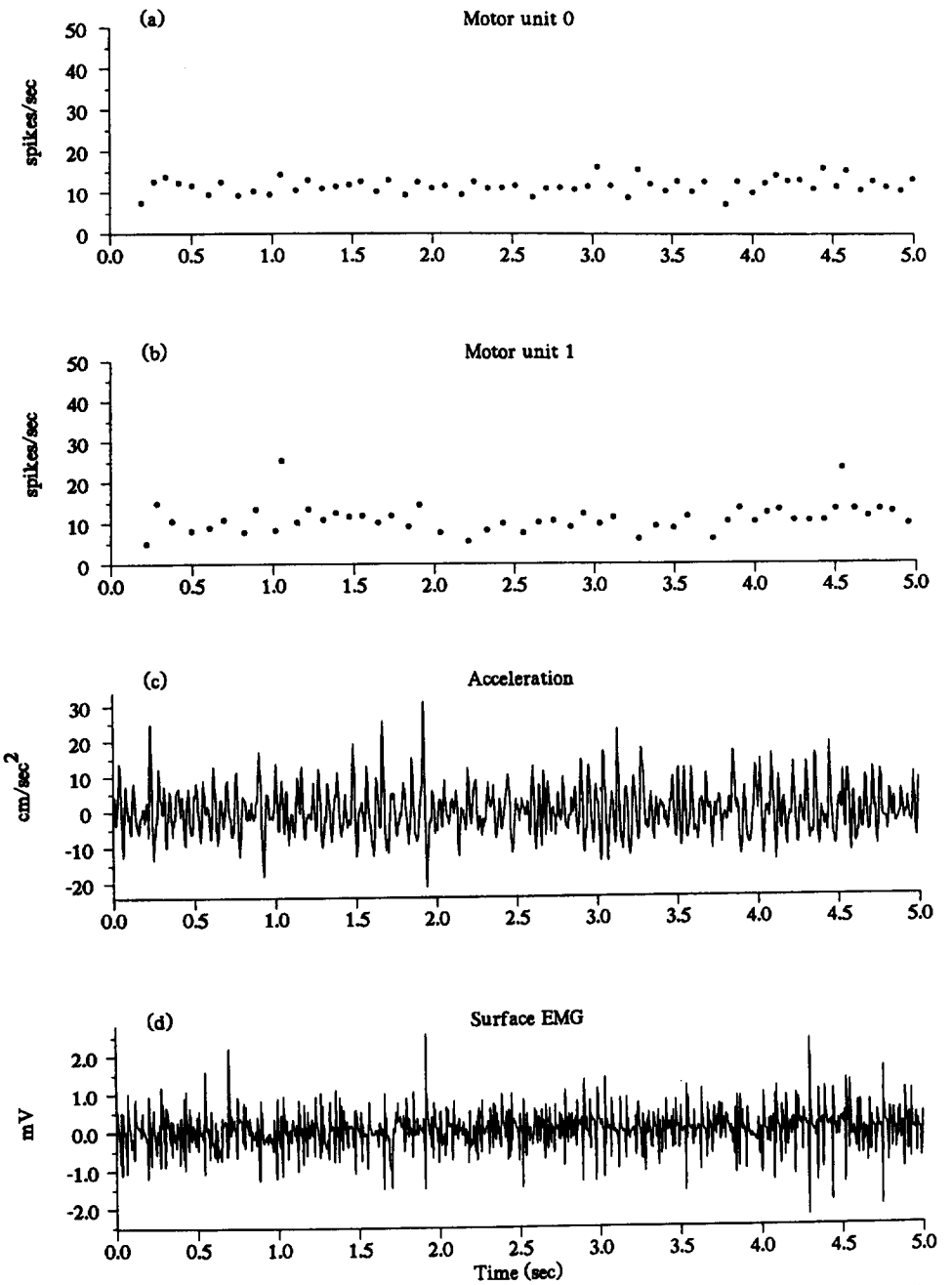

Fig. 1. Five-second segments showing (a) instantaneous frequency of motor unit 0, (b) instantaneous frequency of motor unit 1, (c) finger acceleration signal, and (d) raw surface EMG signal.

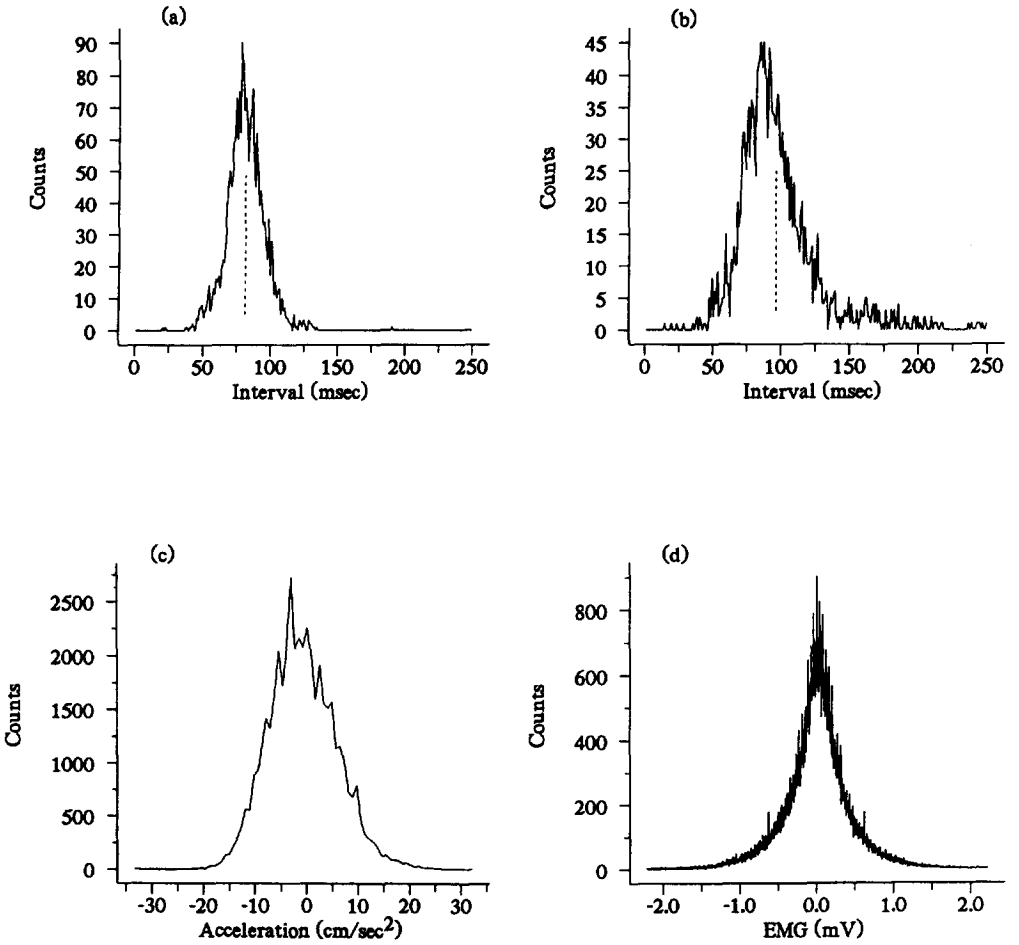

Fig. 2. (a) Interval histogram for motor unit 0 and (b) interval histogram for motor unit 1. Vertical dashed line in (a) and (b) corresponds to the mean firing interval of each motor unit. (c) Amplitude histogram of acceleration record, and (d) amplitude histogram of surface EMG record.

plotted for ±5 standard deviations about the mean. The acceleration signal has a peak value of around 30 cm/sec^2, with a standard deviation or RMS value of 6.67 cm/sec^2.

Physiological tremor is a complex signal resulting from interactions between several neural and mechanical factors (e.g., see Elble and Koller, 1990). The spectrum of physiological tremor contains two types of component identified as distinct peaks in the estimated tremor spectrum. The first component, due in part to the natural resonance of the limb being studied, is sensitive to changes in inertial loading which results in a downward shift of the frequency of the spectral peak with increased inertial loading. This component has been termed the mechanical reflex component of physiological tremor (see Elble and Koller, 1990). The second type of component is referred to as neurogenic, the position of the peak in the tremor spectrum corresponding to this component is not sensitive to changes in inertial loading (Stiles and Randall, 1967).

A frequency domain description of the coupling between discharges from pairs of single motor units has revealed the presence of distinct frequency bands (Farmer *et al.*, 1993), which overlap with the range of frequencies present in finger tremor. The analysis in the present report will concentrate on two particular questions. The first is whether frequency components of motor unit coupling can be associated with a distinct feature of physiological tremor. The second question to be addressed is whether a surface EMG signal can provide information about motor unit coupling, and to what extent the information available from an analysis using single motor unit discharges can be obtained by using a surface EMG signal in the analysis.

III. DEFINITIONS AND ASSUMPTIONS ABOUT THE DATA

The motor unit spike trains are assumed to be realizations of stochastic point processes. A stochastic point process, N, may be defined formally as a random non-negative integer valued measure (Brillinger, 1978) and in practice is represented by the ordered times of occurrence of motor unit spikes. It is assumed that at most one event occurs in a suitably small interval, dt, equivalent to the sampling interval. A point process which satisfies this condition is known as orderly. This assumption is discussed in relation to neuronal spike trains by Conway *et al.* (1993).

The two point processes will be denoted by N_0 for motor unit 0, and N_1 for motor unit 1, respectively. For process N_1, the counting variate $N_1(t)$ counts the number of events in the interval $(0,t]$. In defining point process parameters it is convenient to introduce differential increments. Thus for process N_1 the differential increment, denoted by $dN_1(t)$, is defined as $dN_1(t) = N_1(t,t+dt]$. This counts the number of events in a small interval of duration dt starting at time t, and in practice, since the process is assumed to be orderly, will take on the value 0 or 1 depending on the occurrence of a motor unit spike in the sampling interval dt ($dt = 1$ msec). A similar definition is used for $dN_0(t)$.

The acceleration record is assumed to be a realization of a zero mean time series, denoted by $x(t)$. The surface EMG signal is full wave rectified to remove waveform artefacts from parameter estimates (see Section IV below), this signal is likewise assumed to be a realization of a time series, denoted by $y(t)$. It is assumed that these time series are real valued with sample values defined at equispaced intervals equal to the sampling interval, dt, denoted by x_t and y_t respectively.

Both point process and time series data are assumed to satisfy two further conditions, that of stationarity, and a mixing condition. Stationarity assumes that moments of up to finite order exist and are independent of any translation of the time arguments. For second order (linear) analysis we assume stationarity to second order, this means, for example, that the second order moment between rectified EMG, $y(t)$, and tremor, $x(t)$, given by the product $\{y(t)\, x(t+u)\}$, is a function of u only, and is independent of the value of t. This is also known as wide sense stationarity. For third order analysis we assume third order stationarity.

The mixing condition assumes that differential increments and/or sample values widely spaced in time are statistically independent (Rosenblatt, 1956; see also Brillinger, 1981, 1983). This assumption results in asymptotic normality of parameter estimates, allowing confidence limits to be constructed. In practice most signals encountered in neurophysiology meet this requirement, any dependency within a process and between processes will have a short span due to influences from other sources and random effects. However, if external stimuli are being used in an analysis, deterministic or completely regular series should be avoided since they will violate the mixing condition.

Time series and point processes are defined formally from a statistical viewpoint in Brillinger (1978).

IV. FOUNDATIONS—THE FINITE FOURIER TRANSFORM

In the present report all second order (linear) analyses are performed using estimation procedures where both time and frequency domain parameters are arrived at through spectral estimation techniques. These frequency domain procedures are based on the method of disjoint sections set out in Rosenberg *et al.* (1989) for point process data. The method of disjoint sections results in simple expressions for confidence intervals for parameter estimates. The frequency domain approach allows a wider range of linear interactions to be considered through multivariate analysis, and in some cases multivariate time domain parameters of interest can only be estimated via the frequency domain. This approach also allows common estimation procedures to be used for different types of point process and/or time series interactions.

Using the method of disjoint sections, the complete record, denoted by R, is divided into L non-overlapping disjoint sections each of length T, where $R = LT$. The basic frequency

domain statistic used in the present study is the finite Fourier transform of a segment of length T from each of the four processes x, y, N_0 and N_1 defined previously. Once the L sections from each process have been transformed, spectral estimates are constructed by algebraic combinations of these transforms.

The finite Fourier transform of the l^{th} segment ($l=1, \ldots, L$) from process x at frequency λ is defined as (Brillinger, 1972)

$$d_x^T(\lambda, l) = \int_{(l-1)T}^{lT} x(t)e^{-i\lambda t}\, dt \approx \sum_{t=(l-1)T}^{lT-1} e^{-i\lambda t}x_t \tag{4.1}$$

with a similar definition for $d_y^T(\lambda, l)$. For point process data the finite Fourier transform of a segment of length T from process N_1 is defined as

$$d_{N_1}^T(\lambda, l) = \int_{(l-1)T}^{lT} e^{-i\lambda t}\, dN_1(t) \approx \sum_{(l-1)T \le \tau_j < lT} e^{-i\lambda \tau_j} \tag{4.2}$$

where τ_j are the times of occurrence of the N_1 events. A similar definition holds for $d_{N_0}^T(\lambda, l)$.

Consideration of these two basic statistics at this stage can provide a useful insight into interpretation of estimates of parameters to be introduced in the following sections. For time series x, the statistic (4.1) can be thought of as performing a Fourier decomposition of the sampled waveform into constituent frequency components, which should highlight any distinct periodic components in the data (Brillinger, 1983). The interpretation of (4.1) in the case of the rectified EMG, process y, is more complex. A decomposition of the raw EMG about the mean value zero would contain information about the shapes of the many individual muscle action potentials contained in the surface EMG. In the present study it is the timing of these potentials which is of interest, thus the sampled waveform is rectified before being Fourier transformed. Full wave rectification is used to maximize information about action potential timing, and no time constant or smoothing is associated with the rectification process to preserve the accuracy of timing information. Thus, over the frequency range of interest (<50 Hz), it can be hypothesized that the statistic (4.1) will reflect mainly the timing of action potentials. One of the objects of the present analysis is to determine to what extent this hypothesis is correct.

For point process N_1, the statistic (4.2) can be thought of as performing a correlation between the sinusoids and co-sinusoids of the complex Fourier exponential with the times of occurrence of the N_1 events. The presence or absence of particular periodicities in the spike timings of process N_1 will lead to increased or decreased values of correlation (at the frequency of the periodicity) from that expected by chance alone, which should highlight periodic components in the discharge.

The analysis of stationary processes through the use of Fourier transforms is discussed in Brillinger (1974, 1983). A particular motivation for using this approach in a statistical analysis is that the large sample statistical properties of the Fourier transform of a stationary process are simpler than those of the process itself, and lead to easily managed quantities (Brillinger, 1974, 1983).

V. PARAMETERS OF LINEAR PROCESSES AND THEIR PAIRWISE INTERACTIONS

In this section various parameters are defined, and estimation procedures described for characterizing the processes x, y, N_0 and N_1 and their linear pairwise interactions. The individual processes are characterized by estimates of the power spectrum, or auto-spectrum of each process. The pairwise relationships between the processes are characterized in the frequency domain by estimates of coherence and phase, and in the time domain by estimates of cumulant density functions. Section VI gives results necessary to estimate confidence limits for all parameter estimates.

We use the term hybrid to characterize a parameter that depends on a time series and a

point process. For example, one may define a hybrid cross-spectrum between point process N_1 and time series x, suppressing the dependency on l, as

$$f_{x1}(\lambda) = \lim_{T\to\infty} \frac{1}{2\pi T} E\{d_x^T(\lambda)\overline{d_{N_1}^T(\lambda)}\} \tag{5.1}$$

where the overbar "$^-$" indicates a complex conjugate, and $E\{\ \}$ denotes the averaging operator or mathematical expectation of a random variable. A similar definition holds for the hybrid cross-spectrum $f_{x0}(\lambda)$, by replacing $d_{N_1}^T(\lambda,)$ with $d_{N_0}^T(\lambda)$. For point process data, the cross-spectrum between N_0 and N_1, denoted by $f_{10}(\lambda)$ is defined in an identical manner (Rosenberg *et al.*, 1989) by substitution of the appropriate finite Fourier transforms, and for time series data, $f_{xy}(\lambda)$ can be similarly defined (Brillinger, 1981). A consistent estimate of $f_{x1}(\lambda)$, denoted by $\hat{f}_{x1}(\lambda)$, and estimated using the method of disjoint sections described in Section IV, is given by

$$\hat{f}_{x1}(\lambda) = \frac{1}{2\pi LT} \sum_{l=1}^{L} d_x^T(\lambda, l)\overline{d_{N_1}^T(\lambda, l)} \tag{5.2}$$

with similar expressions for the estimation of the other pairwise cross-spectra, $\hat{f}_{x0}(\lambda)$, $\hat{f}_{10}(\lambda)$ and $\hat{f}_{xy}(\lambda)$.

The auto-spectrum of the process x, $f_{xx}(\lambda)$, is defined and estimated by replacing the subscript N_1 with x in equations (5.1) and (5.2). Similar procedures hold for the other auto-spectra $f_{00}(\lambda)$, $f_{11}(\lambda)$, and $f_{yy}(\lambda)$.

For large T and $\lambda \neq 0$, the estimated cross-spectrum $\hat{f}_{x1}(\lambda)$ may be seen to have the same form as a complex covariance parameter, $\text{cov}\{A,B\} = E\{(A - E\{A\})\overline{(B - E\{B\})}\}$, and can be interpreted as the covariance between the components, at frequency λ, of processes N_1 and x. The estimated auto-spectrum, $\hat{f}_{xx}(\lambda)$, has the same form as a variance parameter and can be interpreted as the variance at frequency λ of the process x (providing an alternative interpretation to that discussed in Section IV). Whereas the RMS and c.o.v. parameters described in Section II can provide an indication of the spread of amplitudes or intervals in the component process, the spectral estimates provide a more comprehensive, and perhaps more useful, characterization of the individual processes by indicating which frequency bands the variance is concentrated in.

One frequency domain measure of association which can be used to assess the linear dependency between processes N_1 and x is the coherence function, written as $|R_{x1}(\lambda)|^2$, and defined, suppressing the dependency on section number l, as

$$|R_{x1}(\lambda)|^2 = \lim_{T\to\infty} |\text{corr}\{d_x^T(\lambda), d_{N_1}^T(\lambda)\}|^2 \tag{5.3}$$

where $\text{corr}\{A,B\}$ denotes the correlation between A and B. Equation (5.3) can be interpreted as the magnitude squared of the correlation between the finite Fourier transforms of processes N_1 and x. The definition of correlation in variance and covariance terms, $\text{corr}\{A,B\} = \text{cov}\{A,B\}/\sqrt{\text{var}\{A\}\text{var}\{B\}}$, leads to an alternative definition of the coherence as

$$|R_{x1}(\lambda)|^2 = \frac{|f_{x1}(\lambda)|^2}{f_{xx}(\lambda)f_{11}(\lambda)} \tag{5.4}$$

(5.4) can be estimated by direct substitution of estimates of the appropriate spectra as

$$|\hat{R}_{x1}(\lambda)|^2 = \frac{|\hat{f}_{x1}(\lambda)|^2}{\hat{f}_{xx}(\lambda)\hat{f}_{11}(\lambda)} \tag{5.5}$$

with other coherence estimates obtained by substitution of the appropriate spectra into an equation similar to (5.5). Coherence functions provide a bounded and normative measure of association, taking on values between 0 and 1, with 0 in the case of independence, and 1 in the case of a perfect linear relationship (Brillinger, 1981; Rosenberg *et al.*, 1989). The

complex valued function $R_{x1}(\lambda)$, whose modulus squared is the coherence, is defined as

$$R_{x1}(\lambda) = \frac{f_{x1}(\lambda)}{\sqrt{f_{xx}(\lambda) f_{11}(\lambda)}}.$$

This function is referred to as the coherency, following Wiener (1930), and can be estimated by direct substitution of spectral estimates in the manner of (5.5). Coherency functions are used in the construction of confidence limits for estimated coherence functions, see Section VI below.

Coherence functions provide estimates of the strength of coupling between two processes. Timing information can be obtained from the phase spectrum, $\Phi_{x1}(\lambda)$, defined as the argument of the cross-spectrum

$$\Phi_{x1}(\lambda) = \arg\{f_{x1}(\lambda)\} \tag{5.6}$$

and can be estimated by

$$\hat{\Phi}_{x1}(\lambda) = \arg\{\hat{f}_{x1}(\lambda)\} \tag{5.7}$$

with the cross-spectrum estimate provided by (5.2). Other phase spectra can be defined and estimated in similar fashion. $\hat{\Phi}_{x1}(\lambda)$ only has a valid interpretation where significant correlation is present between N_1 and x. In practice $|\hat{R}_{x1}(\lambda)|^2$ can be used to indicate these regions, where the phase can be interpreted as the difference between harmonics of N_1 and x at frequency λ. A useful basic model for the interpretation of phase estimates is a pure delay, when the phase curve will be a straight line passing through the origin, with a slope equal to the delay (Jenkins and Watts, 1968; Rosenberg *et al.*, 1989). The argument of the estimated cross-spectrum, (5.7) can be obtained from the arctan function, this will result in a phase estimate over the range $[-\pi/2, \pi/2]$, however, the signs of the real and imaginary parts of $\hat{f}_{x1}(\lambda)$ can be used to determine in which quadrant the arctangent falls, so extending the range to $[-\pi, \pi]$. Where significant coherence is present over a wide range of frequencies it is possible to remove the constraint on the phase and extend the phase estimate outside the range $[-\pi, \pi]$ to avoid discontinuities in phase estimates. This estimate, referred to as the unconstrained phase, is useful in the case of data with time delays between processes. See Brillinger (1981) for a discussion of the representation of phase.

In the time domain, the linear pairwise association between two processes can be characterized by second order cumulant density functions. The second order hybrid cumulant density function between processes N_1 and x, $q_{x1}(u)$, is defined by the inverse Fourier transform of the cross-spectrum $f_{x1}(\lambda)$ following Brillinger (1974) as

$$q_{x1}(u) = \int_{-\pi}^{\pi} f_{x1}(\lambda) e^{i\lambda u} d\lambda \tag{5.8}$$

with similar definitions for the other hybrid cumulant density function $q_{x0}(u)$, the point process cumulant density function $q_{10}(u)$, and the time series cumulant density function $q_{xy}(u)$. The above hybrid cumulant can be estimated by the following expression

$$\hat{q}_{x1}(u) = \frac{2\pi}{T} \sum_{|j| \le T/2} \hat{f}_{x1}(\lambda_j) e^{i\lambda_j u} \tag{5.9}$$

where $\lambda_j = 2\pi j/T$. Estimation of the other cumulant densities, $\hat{q}_{x0}(u)$, $\hat{q}_{10}(u)$ and $\hat{q}_{xy}(u)$ is achieved by substitution of the appropriate cross spectra into eqn (5.9).

Cumulant densities provide a measure of statistical dependence between random processes (Brillinger, 1972; Rosenblatt, 1983; Mendel, 1991). If any of the processes under consideration is independent of the other processes then the value of the cumulant is 0. Cumulant densities can assume either positive or negative values, and in the second order hybrid case they have an interpretation similar to a spike triggered average.

Second order cumulant density functions provide a time domain measure of association between two processes which complements the frequency domain representation provided by coherence functions. However, there are two main differences. Firstly, cumulant density functions are dimensional, i.e. the estimated value depends on the units of measurement. Secondly, cumulant densities are unbounded measures of association which in practice means that, although in the null case of independent processes the asymptotic value is zero, there is no upper limit indicating a perfect linear relationship. These differences are further discussed in Rosenberg *et al.* (1989).

Cumulant density functions can also be defined and estimated directly in the time domain, however estimation of $\hat{q}_{x1}(u)$ via the frequency domain facilitates the construction of confidence limits, see next section.

VI. CONFIDENCE LIMITS FOR ESTIMATES OF PARAMETERS OF LINEAR PROCESSES AND THEIR PAIRWISE INTERACTIONS

In this section we will develop expressions for the variances of the estimated parameters whose estimation procedures are given in the previous section. These will then be used to construct confidence limits for all the parameters. The procedure for estimating such confidence limits involves two steps, firstly the development of an expression for the variance of a particular estimate, and secondly the construction of confidence limits for a desired level of significance. In the present report 95% confidence limits are used. Given an estimate $\hat{z}$ of a parameter z, with an estimate of the asymptotic variance, $\text{var}\{\hat{z}\}$, then under the assumption of asymptotic normality estimates of the upper and lower 95% confidence limits can be obtained by estimating $\pm 1.96(\text{var}\{\hat{z}\})^{1/2}$ about the mean or asymptotic value. The assumption of asymptotic normality of the estimates follows from the mixing condition set out in Section III.

For estimates of the auto-spectrum, $\hat{f}_{xx}(\lambda)$, obtained via (5.2), it can be shown that the variance can be approximated by $\text{var}\{\hat{f}_{xx}(\lambda)\} \approx L^{-1}(f_{xx}(\lambda))^2$, (Bloomfield, 1976), where L is the number of disjoint sections used to estimate the spectrum. This expression contains the value of the actual spectrum at a particular frequency and will therefore change with changing frequency. In situations where the variance of an estimate depends on the parameter being estimated, it is common practice to apply a variance stabilizing transform which results in a function of the estimate whose variance is independent of the value of the original estimate. (e.g., see Jenkins and Watts, 1968, Ch. 3). The appropriate transform in this case is the logarithmic transform, giving the simplified expression $\text{var}\{\ln(\hat{f}_{xx}(\lambda))\} \approx L^{-1}$. It is customary practice to plot spectra on a $\log_{10}$ scale, giving

$$\text{var}\{\log_{10}(\hat{f}_{xx}(\lambda))\} = (\log_{10}(e))^2 L^{-1} \tag{6.1}$$

with a resulting estimate and 95% confidence limits at frequency λ of

$$\log_{10}(\hat{f}_{xx}(\lambda)) \pm 0.851 L^{-1/2} \tag{6.2}$$

An identical procedure holds for $\hat{f}_{yy}(\lambda)$.

The asymptotic value of the auto-spectrum of the point process N_1 as $\lambda \to \infty$ is $P_1/2\pi$ (Bartlett, 1963), in the case of a random or Poisson point process the spectrum is identically equal to this value (Bartlett, 1963). P_1 is the mean intensity of the point process N_1, which can be estimated as $N_1(R)/R$, where R is the record length. This allows an asymptotic value and upper and lower 95% confidence limits to be estimated for the log transform of the estimated point process spectrum $\hat{f}_{11}(\lambda)$ as

$$\log_{10}\left(\frac{\hat{P}_1}{2\pi}\right) \pm 0.851 L^{-1/2} \tag{6.3}$$

An identical procedure holds for $\hat{f}_{00}(\lambda)$.

Following Brillinger (1981) and Rosenberg *et al.* (1989) the variance of the hybrid coherence estimate (5.5) can be approximated by

$$\mathrm{var}\{|\hat{R}_{x1}(\lambda)|^2\} = \frac{2}{L}|R_{x1}(\lambda)|^2[1-|R_{x1}(\lambda)|^2]^2 \tag{6.4}$$

This expression contains the coherence at each frequency λ, the estimated value (5.5) can be substituted into this expression allowing upper and lower 95% confidence limits about the estimated value to be constructed. Alternatively a variance stabilizing transform can be used, as above. The appropriate variance stabilizing transform is the arctanh transformation of the modulus of the coherency function (Jenkins and Watts, 1968; Brillinger, 1981; Rosenberg *et al.*, 1989) leading to the expression

$$\mathrm{var}\{\mathrm{Tan}h^{-1}|\hat{R}_{x1}(\lambda)|\} = \frac{1}{2L} \tag{6.5}$$

Thus approximate 95% confidence limits for $\mathrm{Tan}h^{-1}|\hat{R}_{x1}(\lambda)|$ at frequency λ are given by $\mathrm{Tan}h^{-1}|\hat{R}_{x1}(\lambda)| \pm 1.96/\sqrt{2L}$. The values in this expression can be transformed back to the domain of $|R_{x1}(\lambda)|^2$ to give 95% confidence limits for $|\hat{R}_{x1}(\lambda)|^2$ at frequency λ. This latter method is used in the present report, and is preferred to the use of (6.4), since variance stabilizing transforms generally produce random variates which are closer to the Normal distribution (Jenkins and Watts, 1968). In the case of independence, $|R_{x1}(\lambda)|^2 = 0$, expressions (6.4) and (6.5) are invalid (Bloomfield, 1976), and therefore also give poor approximations for small values of coherence. In this case the distribution of $|\hat{R}_{x1}(\lambda)|^2$ can be evaluated in terms of the incomplete Beta function with parameters 1 and $(L-1)$ (Bloomfield, 1976; Brillinger, 1981). The confidence limit at the $100\alpha\%$ point is given by $1-(1-\alpha)^{1/(L-1)}$. Thus it is necessary to include the line

$$1-(0.05)^{1/(L-1)} \tag{6.6}$$

on a coherence plot as an estimate of the upper 95% confidence limit under the hypothesis of independence. Estimated values of coherence lying below this line can be taken as evidence for the lack of a linear association between the two processes, i.e. that zero coherence is plausible at that frequency. These procedures hold for all the coherence functions defined above.

Following Brillinger (1981) and Rosenberg *et al.* (1989), the variance of the phase estimate, $\hat{\Phi}_{x1}(\lambda)$, can be shown to be

$$\mathrm{var}\{\hat{\Phi}_{x1}(\lambda)\} = \frac{1}{2L}\left(\frac{1}{|R_{x1}(\lambda)|^2}-1\right) \tag{6.7}$$

where L is the number of disjoint sections averaged in the cross spectral estimate (5.2). The estimated phase (5.7) is approximately normally distributed when the coherence is not small (Bloomfield, 1976), and in practice the estimated coherence can be substituted into the above equation giving a resultant phase estimate and upper and lower 95% confidence limit of

$$\hat{\Phi}_{x1}(\lambda) \pm 1.96\left[\frac{1}{2L}\left(\frac{1}{|\hat{R}_{x1}(\lambda)|^2}-1\right)\right]^{1/2} \tag{6.8}$$

Similar procedures hold for phase spectra derived from the other cross spectra defined above.

In the present report, the setting of confidence limits for estimates of cumulant density functions uses the same integral procedure given in Conway *et al.* (1993), following Rigas (1983). The variances of the second order point process cumulant density and second order hybrid cumulant density function have been defined in Rigas (1983), under the assumption of independence. The variance of the hybrid cumulant density estimate (5.9) can be approximated by

$$\text{var}\{\hat{q}_{x1}(u)\} \approx \frac{2\pi}{R} \int_{-\pi}^{\pi} f_{xx}(\lambda) f_{11}(\lambda) d\lambda \tag{6.9}$$

where R is the record length, and $f_{xx}(\lambda)$ and $f_{11}(\lambda)$ are the auto-spectra of the component processes. A similar expression holds for the other second order cumulant density functions defined above. In practice this expression can be estimated using a discrete summation and substitution of auto-spectra based on (5.2) into equation (6.9). The appropriate expression to estimate the variance is then

$$\text{var}\{\hat{q}_{x1}(u)\} \approx \left(\frac{2\pi}{R}\right)\left(\frac{2\pi}{T}\right) \sum_{j=1}^{T/2-1} 2\hat{f}_{xx}(\lambda_j)\hat{f}_{11}(\lambda_j) \tag{6.10}$$

where $\lambda_j = 2\pi j/T$, R is the record length, and T is the segment length used in the estimation of the finite Fourier transforms (4.1) and (4.2). This expression is based on the assumption of two independent processes, the value of the cumulant in this case is zero. Under this hypothesis the asymptotic value and upper and lower 95% confidence limits for the estimated cumulant (5.9) are given by

$$0 \pm 1.96\left[\left(\frac{2\pi}{R}\right)\left(\frac{2\pi}{T}\right) \sum_{j=1}^{T/2-1} 2\hat{f}_{xx}(\lambda_j)\hat{f}_{11}(\lambda_j)\right]^{1/2} \tag{6.11}$$

Expressions (6.9) to (6.11) are valid for other cumulant densities defined above, by substitution of the appropriate spectra. Estimated values of the cumulant lying inside these limits can be taken as evidence for the lack of a linear association between the two processes at a particular lag u.

VII. EXAMPLES OF PARAMETERS OF LINEAR PROCESSES AND THEIR PAIRWISE INTERACTIONS

All the parameters in this section have been estimated using a segment length of T = 1024 points in the finite Fourier transforms (4.1) and (4.2). This defines the minimum frequency which can be resolved (and thus the spectral resolution) according to the relationship $\Delta f = 1/(T\ dt)$ Hz, where dt is the sampling interval for the data set. Here dt = 1 msec, this gives a spectral resolution of $\Delta f = 0.976$ Hz. The data set is 180 sec in duration, R = 180 000, giving the number of complete segments as L = 175.

A brief description of the data set along with amplitude and interval statistics was given in Section II. As outlined in Section V, a more revealing analysis of the structure within each process can be undertaken by examining estimates of the auto-spectra. Estimates of the log spectrum of the four processes under consideration are shown in Fig. 3, based on (5.2). With L = 175, the approximate 95% confidence limits as defined in (6.2) and (6.3) are ±0.0643 dB. These are marked on the graphs in an appropriate fashion.

In Fig. 3a, b are shownwpoint p ocess spectral estimates for each of the two motor units, $\hat{f}_{00}(\lambda)$ and $\hat{f}_{11}(\lambda)$, along with the asymptotic values for a random discharge with the same mean rates and upper and lower 95% confidence limits, derived from (6.3). The dominant feature in each spectrum is a large peak at 12 Hz for motor unit 0 and at 11 Hz for motor unit 1, representing the mean rate of discharge of the motor units. Motor unit 0 has a more regular discharge, as indicated by the lower c.o.v., resulting in a more clearly defined spectral peak and more obvious harmonic components in Fig. 3a than 3b.

In Fig. 3c, d are shown time series spectral estimates of the acceleration record, $\hat{f}_{xx}(\lambda)$, and the rectified EMG, $\hat{f}_{yy}(\lambda)$. The 95% confidence interval for the estimate, derived from the second term in (6.2), is indicated by the solid vertical line in the top right of each graph. These lines are 0.1286 dB in magnitude and provide a scale bar against which to assess the significance of distinct features in each estimate. Comparison with this scale bar shows the tremor spectrum (Fig. 3c) contains three distinct frequency bands. The dominant feature is centred about 20 Hz, this is the mechanical reflex component of physiological tremor

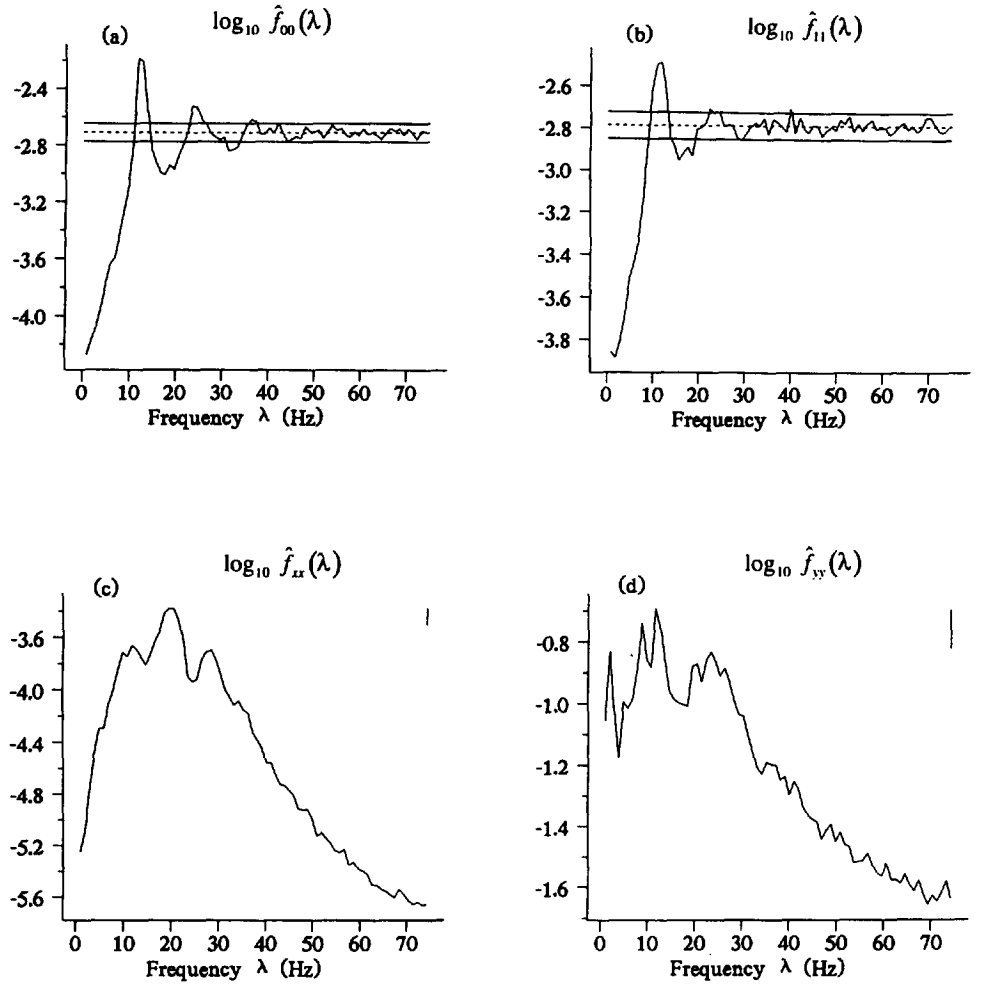

Fig. 3. Log plots of (a) estimated point process auto-spectrum of motor unit 0, $\hat{f}_{00}(\lambda)$, and (b) estimated point process auto-spectrum of motor unit 1, $\hat{f}_{11}(\lambda)$. Dashed horizontal lines represent the asymptotic value of each estimate, solid horizontal lines represent the upper and lower 95% confidence limits. Log plots of (c) estimated time series auto-spectrum of tremor signal, $\hat{f}_{xx}(\lambda)$, and (d) estimated time series auto-spectrum of rectified surface EMG signal, $\hat{f}_{yy}(\lambda)$. Solid vertical lines at the top right represent the 95% confidence interval for each estimate.

(Stiles and Randall, 1967). The other two components centred at 11 Hz and 28 Hz are neurogenic components (Stiles and Randall, 1967; Amjad *et al.*, 1994b) whose frequency does not change with loading. The spectral estimate for the rectified EMG (Fig. 3d) has two dominant features, with power concentrated in frequency bands at 8–12 Hz and 20–30 Hz, indicating either (1) a significant modulation of the timing of individual motor unit spikes, or (2) a concentration of intervals corresponding to these frequencies. Comparison with the interspike interval histograms in Fig. 2a, b, shows that the 8–12 Hz component could result from either mechanism, but the 20–30 Hz component is likely to be a modulation effect, because of the almost complete absence of any intervals corresponding to these frequencies in the two observed motor units.

The linear pairwise interactions between the signals are characterized in the frequency domain by coherence estimates (5.5) shown in Fig. 4. Within the context of the present report there are four relevant interactions, these are the motor unit–motor unit, $|\hat{R}_{10}(\lambda)|^2$, the two motor unit–tremor, $|\hat{R}_{x0}(\lambda)|^2$ and $|\hat{R}_{x1}(\lambda)|^2$, and the surface EMG–tremor, $|\hat{R}_{xy}(\lambda)|^2$, interactions. Also shown in each coherence estimate is the upper 95% confidence limit based on the assumption of independence, given by (6.6). For $L = 175$ this has the value 0.0170, and is indicated by the horizontal dashed line in each graph.

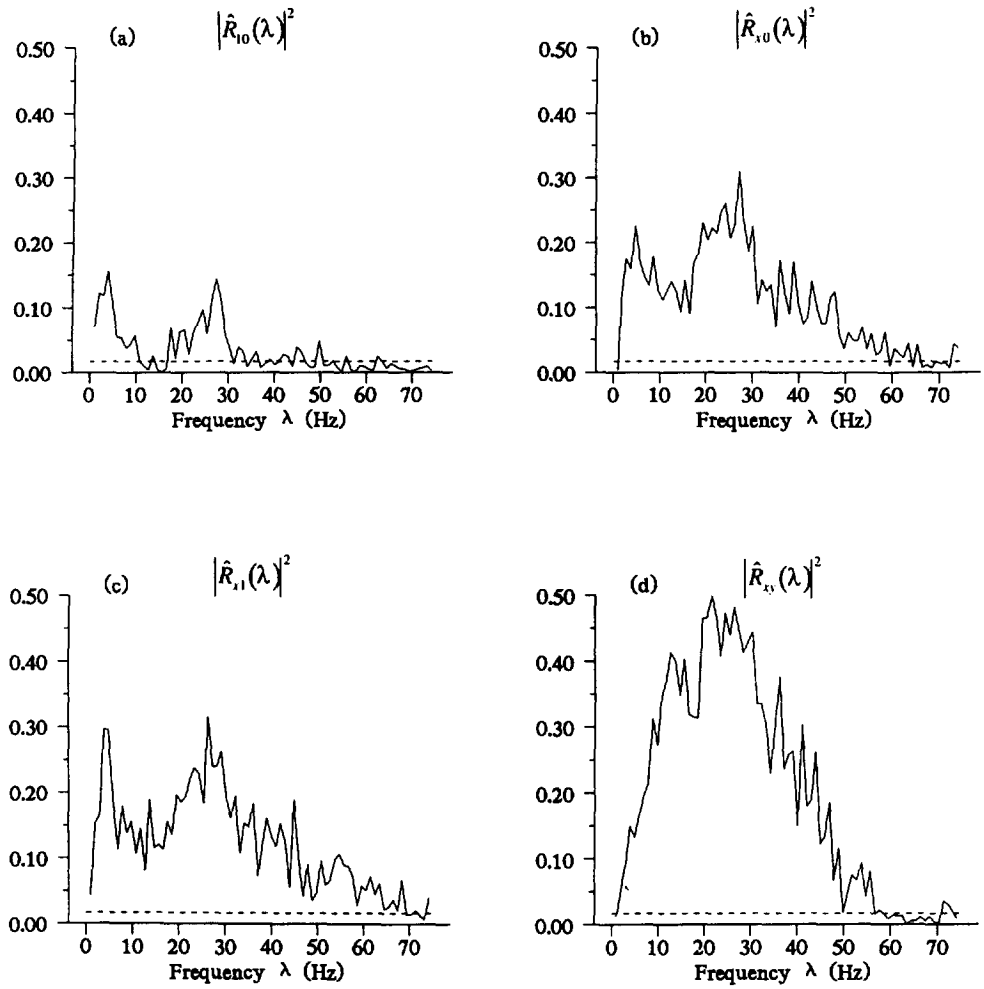

Fig. 4. Estimated coherence between (a) motor unit 0 and motor unit 1, $|\hat{R}_{10}(\lambda)|^2$, (b) motor unit 0 and tremor, $|\hat{R}_{x0}(\lambda)|^2$, (c) motor unit 1 and tremor, $|\hat{R}_{x1}(\lambda)|^2$, and, (d) surface EMG and tremor, $|\hat{R}_{xy}(\lambda)|^2$. The horizontal dashed line in each graph represents an estimate of the upper 95% confidence limit based on the assumption of independence.

The coherence estimates show a progression of increasing magnitude with the different types of interaction. The motor unit–motor unit coherence is the weakest and has two distinct bands around 5 Hz and 20–30 Hz. This mirrors the findings of Farmer *et al.* (1993) who studied motor unit coupling in human 1DI muscles. Both these frequency bands represent periodicities outside the range of intervals present in the interval histograms (Fig. 2a, b) indicating common modulation as the source of this coupling. Farmer *et al.* (1993) proposed that these two frequency bands in coherence estimates were due to separate mechanisms, with a 16–32 Hz component due in part to activity in common descending inputs to motoneurons.

The coherence estimates between the two motor units and the tremor (Fig. 4b, c) similarly suggest that coupling occurs in two frequency bands which are centred around the same frequencies as in Fig. 4a, around 5 Hz and 20–30 Hz. The strength of coherence and range of significant frequencies are larger than in Fig. 4a, indicating stronger interactions. The estimated coherence between the surface EMG and tremor is the strongest of the four interactions, and has a similar range of frequencies of significant values to the motor unit–tremor coherence estimates. This would seem to indicate that the surface EMG is a useful predictor for determining what frequency components in motor unit discharges are coupled to finger tremor, however the relative magnitude of the estimate in Fig. 4d perhaps does not appear to be as strong around 5 Hz in comparison to

Fig. 4b and c. This will be discussed further when considering the multivariate parameters. Comparison of the motor unit–tremor coherences with the autospectral estimates in Fig. 3 shows that the strongest coupling is not at the fundamental frequency of the motor units (11–12 Hz), in fact this frequency represents the minimum coherence value between the two maxima at 5 and 25 Hz. From this we can conclude that the frequency component which represents the main periodicity in the individual motor units discharges makes the smallest contribution to physiological tremor over the range 0 to about 30 Hz. This is further explored for a range of incremental loadings in Conway *et al.* (1995).

In Fig. 5a, b, are re-plotted the two coherence estimates from Fig. 4a, d, respectively, along with the estimated 95% confidence limits for each estimate, based on the inverse transformation of (6.5). From Fig. 5a we can see that the motor unit–motor unit coherence estimate has a peak value of 0.156 ± 0.07 at 3.9 Hz, and 0.144 ± 0.068 at 27.3 Hz. The EMG–tremor coherence estimate has a peak value of 0.50 ± 0.073 at 21.5 Hz. Over the range of estimated peak coherences in Fig. 4, the confidence interval is of reasonably constant width at about ± 0.07. In percentage terms, the two peaks in Fig. 5a have estimated values of around $0.15 \pm 47\%$. Expressed in this form it is clear that care should be exercised in the interpretation of any apparent fine detail in these coherence

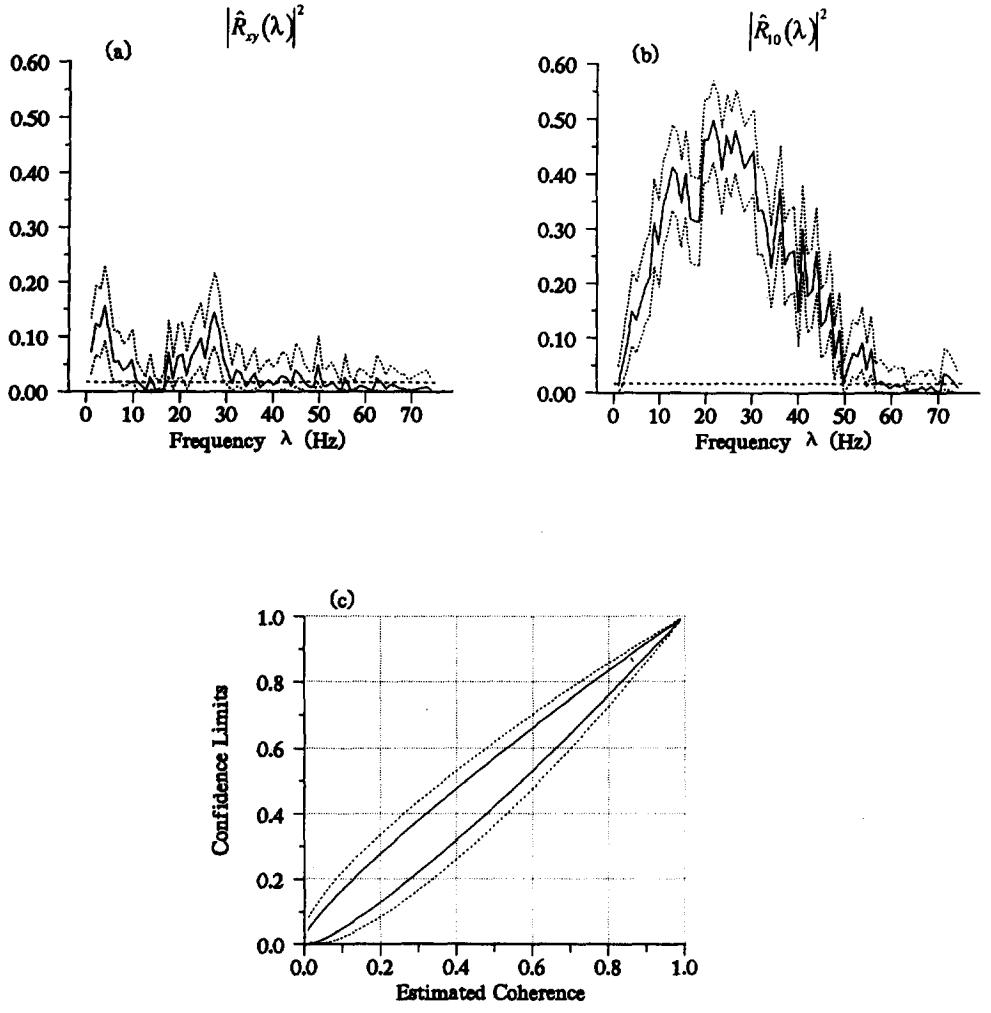

Fig. 5. (a) Coherence estimate of Fig. 4a, $|\hat{R}_{10}(\lambda)|^2$, with upper and lower 95% confidence limits at each frequency included as dotted lines. (b) Coherence estimate of Fig. 4d, $|\hat{R}_{xy}(\lambda)|^2$, with upper and lower 95% confidence limits at each frequency included as dotted lines. (c) Graph of estimated coherence versus 95% confidence limits for L = 175 segments (continuous lines) and L = 58 segments (dotted lines).

estimates. Fig. 5c provides a summary graph of the estimated coherence vs upper and lower 95% confidence limit, based on the back transformation of equation (6.5), for two values of L. The solid lines correspond to the present analysis, L = 175, the two dotted lines are for L = 58 (the number of segments for a data set of 60 seconds, with dt = 1 msec and 1 Hz resolution: R = 60 000 and T = 1024). This graph can be used to obtain confidence limits for coherence estimates constructed using the method of disjoint sections described above. For example an estimated coherence of 0.2 has a 95% confidence interval of [0.129, 0.278] for L = 175, while for L = 58 it is [0.084, 0.337].

The four phase estimates, corresponding to the interactions in Fig. 4, are shown in Fig. 6 plotted in unconstrained form. The phase estimate between the two motor units, $\hat{\Phi}_{10}(\lambda)$ in Fig. 6a, is dominated by the delay between the two spike trains. Closer inspection of this phase estimate suggests that the slope of the phase may be slightly different in the two sections where the coherence is significant, this can be further investigated by application of the weighted least squares regression analysis outlined in Rosenberg *et al.* (1989, Appendix) to estimate the slope of the phase curve and thus the delay in each of the two sections. Application of this analysis gives a delay of 12.76 ± 3.09 msec for an 11-point analysis from 0.97 to 10.74 Hz, and a delay of 4.17 ± 0.69 msec for a 15-point analysis from 17.57 to 31.25 Hz. These estimates are for a regression analysis involving a 95% confidence interval

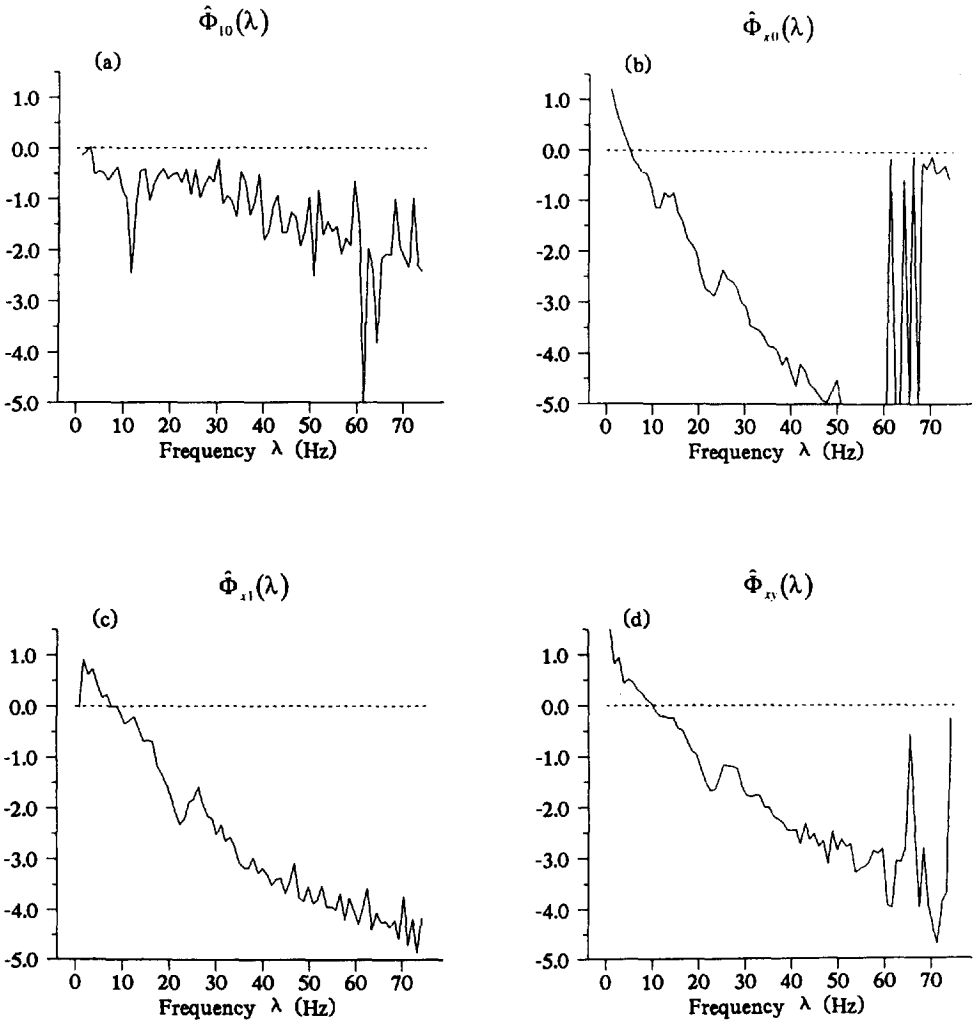

Fig. 6. Estimated phase between (a) motor unit 0 and motor unit 1, $\hat{\Phi}_{10}(\lambda)$, (b) motor unit 0 and tremor, $\hat{\Phi}_{x0}(\lambda)$, (c) motor unit 1 and tremor, $\hat{\Phi}_{x1}(\lambda)$ and, (d) surface EMG and tremor, $\hat{\Phi}_{xy}(\lambda)$. Phase estimates are plotted in unconstrained form.

based on the assumption of normality. At this level of confidence the null hypotheses of the same delay is rejected, which helps to reinforce the suggestion that the frequency bands reflect different neurophysiological processes. These two sections from the original phase estimates are re-plotted in Fig. 7a, along with dashed lines representing the estimated delays. Also included are the 95% confidence limits, (6.8), shown as dotted lines.

For the three phase estimates in Fig. 6b, c and d, which are similar in form, estimation of any delay over the range of significant coherence is not appropriate, since these estimates all deviate markedly from the pure delay phase model at low frequencies. Closer inspection of these phase estimates indicates a shift at higher frequencies towards a straight line which passes through the origin when extrapolated back. The region from 18–50 Hz appears to fit the model for a pure delay, and regression analysis based on a 33-point section in this range yields delays of 16.8 ± 0.42 msec, 12.7 ± 0.44 msec and 9.1 ± 0.41 msec for $\hat{\Phi}_{x0}(\lambda)$, $\hat{\Phi}_{x1}(\lambda)$ and $\hat{\Phi}_{xy}(\lambda)$ respectively. This section from $\hat{\Phi}_{x0}(\lambda)$, is re-plotted in Fig. 7b along with the fitted regression line and 95% confidence limits for the original phase estimate, these can be seen to narrow with increasing values of estimated coherence. In the region 20–30 Hz the regression line lies outside these confidence limits, thus the pure delay model may not be valid in these regions as well as at lower frequencies. Similar comments apply to $\hat{\Phi}_{x1}(\lambda)$ and $\hat{\Phi}_{xy}(\lambda)$. The matching of only part of the phase estimate to a pure delay may indicate different mechanisms in the coherence estimates (Fig. 4b–d) operating in different frequency bands. An alternative interpretation of these three phase estimates is discussed in a linear systems context in Section XIII.

The four second order cumulant density estimates are shown in Fig. 8. The point process cumulant density estimate plotted for lag values of ± 50 msec, and the hybrid and time series cumulant density estimates are plotted for lag values of ± 250 msec. The estimated point process cumulant in Fig. 8a, $\hat{q}_{10}(u)$, illustrates short-term synchrony between the two motor unit discharges, with a central peak of around 10 msec in width. The latency of the peak occurs at about 4 msec, in agreement with the delay estimated from the phase. Note that the central peak does not extend to the latency of 12 msec obtained from the low frequency region of the phase. This suggests that the central peak may represent in part the higher frequency band present in the coherence. Small sidebands are present, these are taken to represent the mapping to the motoneuron discharges of periodic structure present in the common inputs responsible for the short-term synchrony

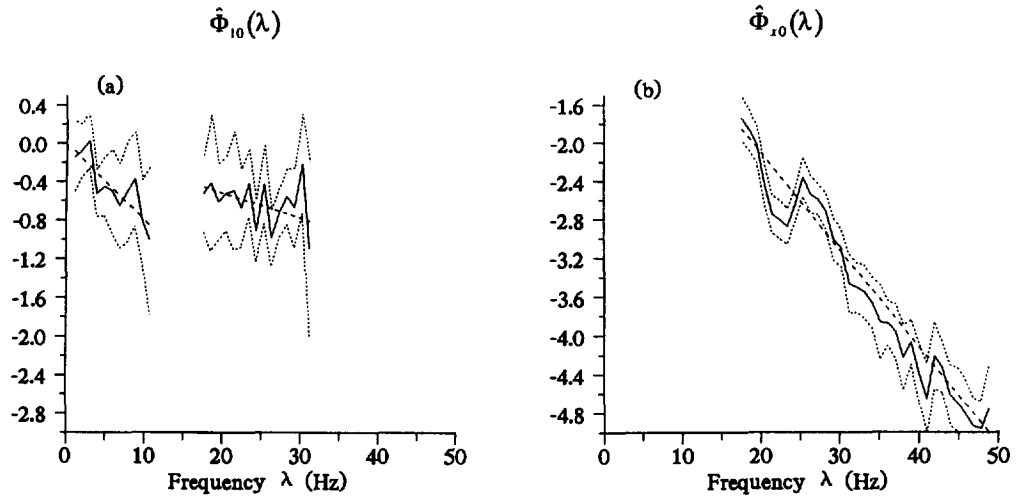

Fig. 7. Sections from the phase estimates in Fig. 6a, b, re-plotted where the corresponding coherence estimates (Fig. 4) are significant, and where a regression analysis could be performed to estimate the delay between the two processes. The fitted regression line is shown as the dashed line through each phase section. The dotted lines in each graph represent an upper and lower 95% confidence limit for each phase estimate at each frequency. Estimated phase between (a) motor unit 0 and motor unit 1, $\hat{\Phi}_{10}(\lambda)$, with estimated delays of 12.11 ± 3.29 msec and 4.14 ± 0.56 msec, and, (b) motor unit 0 and tremor $\hat{\Phi}_{x0}(\lambda)$, with an estimated delay of 16.8 ± 0.42 msec.

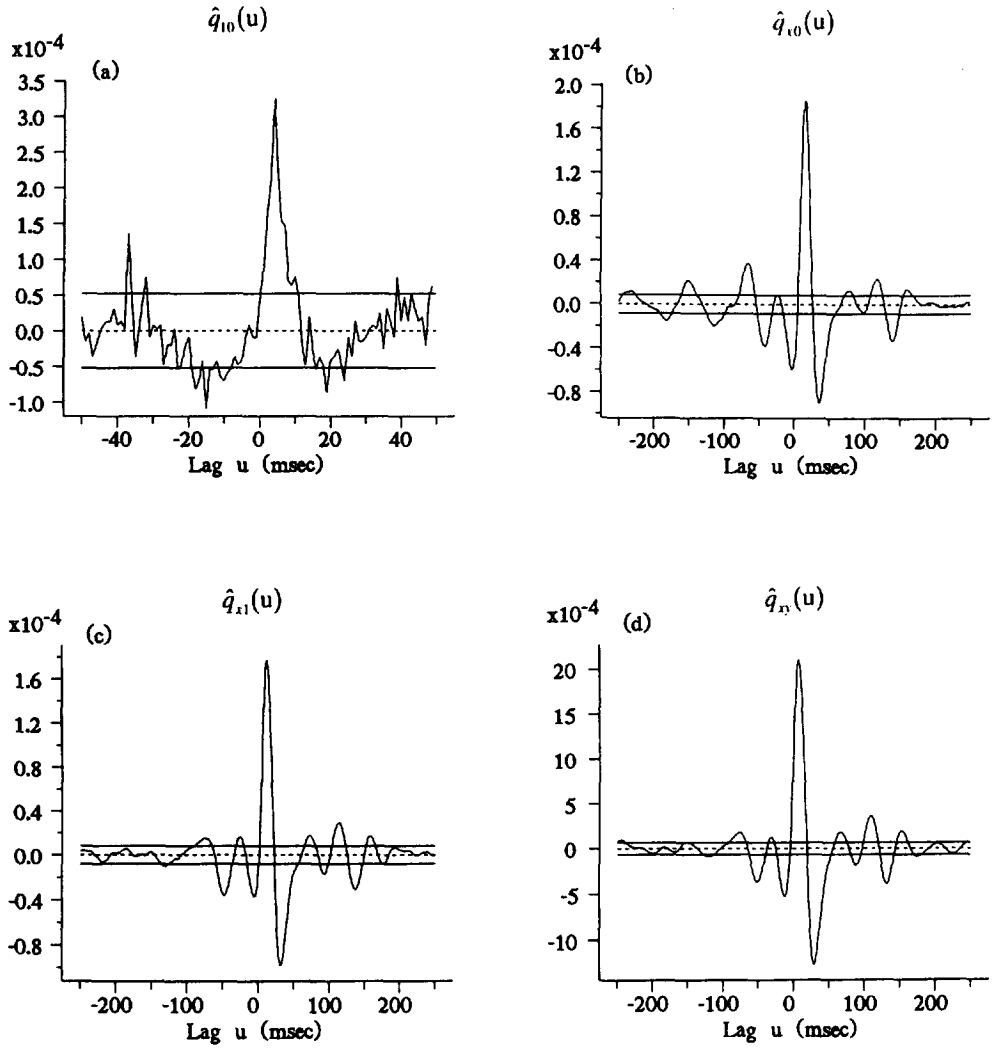

Fig. 8. Estimated cumulant density between (a) motor unit 0 and motor unit 1, $\hat{q}_{10}(u)$, (b) motor unit 0 and tremor, $\hat{q}_{x0}(u)$, (c) motor unit 1 and tremor, $\hat{q}_{x1}(u)$, and, (d) surface EMG and tremor, $\hat{q}_{xy}(u)$. The horizontal lines in each graph show the asymptotic value (dashed line at zero) and estimated upper and lower 95% confidence limits based on the assumption of independence.

(Moore *et al.*, 1970). In this case the interval from the peak at 4 msec to each sideband is around 35 msec, this represents a periodicity of 29 Hz, which is consistent with the coherence estimate in Fig. 4a.

The estimated cumulants of the effects of the motor units and EMG onto the finger acceleration illustrate a clear organization of the tremor signal before and after time zero. In these figures the reference at time zero corresponds to motor unit or surface EMG activity. The two hybrid cumulant densities, $\hat{q}_{x0}(u)$ and $\hat{q}_{x1}(u)$, (Fig. 8b, c) have the advantage of an interpretation similar to a spike triggered average where time zero represents the time of occurrence of a motor unit spike. The main feature in each graph is the large peak following each motor unit spike. This feature represents the acceleration response to motor unit pulses and has the form of a damped oscillation. One of the main components of this part of the response will be the representation in the acceleration record of the mechanical reflex response to motor unit twitches.

The time series cumulant estimate in Fig. 8d, $\hat{q}_{xy}(u)$, has a similar time-course to both the hybrid cumulant estimates, which suggests that the time series cumulant extracts the same features from the tremor record as the hybrid cumulant estimates. This result taken with the previous comments relating to the coherence estimates in Fig. 4 would seem to

indicate that the surface EMG when used in this way acts as a powerful predictor of pooled motor unit activity within the muscle.

The hybrid cumulant in Fig. 8b has eight maxima above the upper 95% confidence limit, these are located at latencies of −232, −151, −65, −23, +16, +80, +119 and +160 msec. The estimate in Fig. 8c has six maxima located at −76, −25, +12, +73, +114 and +158 msec. Similarly the time series estimate in Fig. 8d has six maxima at −75, −31, +8, +67, +110 and +153 msec. The timing of the first peak after time zero matches the delay estimated by regression analysis for the range 18–50 Hz from the phase plots, which indicates that this frequency band is involved in this part of the response. Comparison with the tremor auto-spectrum estimate in Fig. 3c shows that this is the range which encompasses both the dominant peak in the spectrum, which was attributed to the mechanical reflex component, as well as the higher frequency neurogenic component around 30 Hz.

Other factors contributing to the time-course of these cumulant density estimates will include tremor–motor unit interactions occurring in different frequency bands, as well as the mapping of periodicities in the signals to the cumulants. For example, the last three significant peaks in the estimated cumulants in Fig. 8b–d are separated by an interval of around 42 msec suggesting a component at 24 Hz. Further insight can be gained by application of linear systems analysis, see Section XI. Analysis using the method of complex demodulation to estimate the magnitude and phase of frequency components present in these hybrid and time series cumulant estimates may also help to identify the origin of features present in these cumulant estimates.

VIII. MULTIVARIATE LINEAR PARAMETERS

With several simultaneously recorded signals, the possibility exists to explore in more detail the relationships between these processes. One method of further exploring the interactions between processes is to use a multivariate linear framework to investigate the dependency between more than two simultaneously recorded signals. Frequency domain methods are particularly advantageous in this respect. They draw largely on regression analysis, and the whole apparatus of multivariate analysis then becomes available for the analysis of the interactions between several processes. This framework is extensively developed for the time series case in Brillinger (1981), and is set out, with many examples, for point process data in Rosenberg *et al.* (1989). We now extend this framework to include hybrid data. This extension follows in a straightforward manner from the procedures developed in Section V.

The first order partial coherence between processes N_1 and x taking into account the common linear effect of process y, $|R_{x1/y}(\lambda)|^2$, can be defined, suppressing the dependencies on λ and l, as

$$|R_{x1/y}|^2 = \lim_{T\to\infty} \left| \mathrm{corr}\left\{ d_x^T - \left(\frac{f_{xy}}{f_{yy}}\right) d_y^T,\ d_{N_1}^T - \left(\frac{f_{1y}}{f_{yy}}\right) d_y^T \right\} \right|^2 \tag{8.1}$$

Estimates of this parameter test the hypothesis that any observed coupling between N_1 and x is entirely due to the common influence of process y, in which case the parameter will have the value zero. Expression (8.1) can be seen to be the magnitude squared of the correlation between the finite Fourier transforms of N_1 and x after removing any linear contribution that process y makes to each of these processes. Expression (8.1) can be expanded and written in terms of ordinary coherence functions as

$$|R_{x1/y}(\lambda)|^2 = \frac{|R_{x1}(\lambda) - R_{xy}(\lambda)R_{y1}(\lambda)|^2}{\left(1 - |R_{xy}(\lambda)|^2\right)\left(1 - |R_{y1}(\lambda)|^2\right)} \tag{8.2}$$

where terms in the numerator are the coherency functions, defined previously (Section V).

The partial cross-spectrum between N_1 and x taking into account process Y, $f_{x1/y}(\lambda)$, can be defined as

$$f_{x1/y}(\lambda) = f_{x1}(\lambda) - \frac{f_{xy}(\lambda) f_{y1}(\lambda)}{f_{yy}(\lambda)} \tag{8.3}$$

The partial auto-spectra, $f_{xx/y}(\lambda)$ and $f_{11/y}(\lambda)$, can also be defined using (8.3) by making the appropriate change in the subscripts. These partial spectra then lead to an alternative definition of the first order partial coherence function by analogy with (5.4) as

$$|R_{x1/y}(\lambda)|^2 = \frac{|f_{x1/y}(\lambda)|^2}{f_{xx/y}(\lambda) f_{11/y}(\lambda)} \tag{8.4}$$

The correspondence between (8.2) and (8.4) may be verified by expanding (8.2) in terms of auto-spectra and cross spectra. The first order partial phase may be defined as

$$\Phi_{x1/y}(\lambda) = \arg\{f_{x1/y}(\lambda)\} \tag{8.5}$$

This function provides information about the timing relation of any residual coupling between N_1 and x after the removal of the common effects of process y.

Estimation of the above quantities follows in a similar fashion to the procedures set out in Section V by direct substitution of estimates of the appropriate spectra. For example, the first order partial cross-spectrum, $\hat{f}_{x1/y}(\lambda)$, can be estimated by

$$\hat{f}_{x1/y}(\lambda) = \hat{f}_{x1}(\lambda) - \frac{\hat{f}_{xy}(\lambda)\hat{f}_{y1}(\lambda)}{\hat{f}_{yy}(\lambda)} \tag{8.6}$$

and similarly the first order partial auto-spectrum, $f_{11/y}(\lambda)$, by

$$\hat{f}_{11/y}(\lambda) = \hat{f}_{11}(\lambda) - \frac{|\hat{f}_{1y}(\lambda)|^2}{\hat{f}_{yy}(\lambda)} \tag{8.7}$$

with $\hat{f}_{xx/y}(\lambda)$ following similarly. First order partial coherence and phase functions can then be estimated as

$$|\hat{R}_{x1/y}(\lambda)|^2 = \frac{|\hat{f}_{x1/y}(\lambda)|^2}{\hat{f}_{xx/y}(\lambda)\hat{f}_{11/y}(\lambda)} \tag{8.8}$$

and

$$\hat{\Phi}_{x1/y}(\lambda) = \arg\left\{\hat{f}_{x1/y}(\lambda)\right\} \tag{8.9}$$

Time domain point process partial parameters can not be directly estimated from the data, but must be determined via the frequency domain. Time domain point process partial parameters are discussed in Brillinger (1975a) and in Abdulaziz *et al.* (1992) who defined the first order point process partial cumulant density as the inverse Fourier transform of the partial cross-spectrum. Following this we define the first order partial cumulant between processes N_1 and x after removal of process y as

$$q_{x1/y}(u) = \int_{-\pi}^{\pi} f_{x1/y}(\lambda) e^{i\lambda u} d\lambda \tag{8.10}$$

This function provides a measure of the time dependency between processes N_1 and x after removal of any common linear influence of process y. An estimation procedure follows from (5.9) as

$$\hat{q}_{x1/y}(u) = \frac{2\pi}{T} \sum_{|j| \le T/2} \hat{f}_{x1/y}(\lambda_j) e^{i\lambda_j u} \tag{8.11}$$

where $\lambda_j = 2\pi j/T$. Similar procedures are applicable to the time series case.

The first order multiple coherence of the combined linear effects of processes N_1 and y onto process x, $|R_{x \cdot 1y}(\lambda)|^2$, can be defined as

$$|R_{x\cdot 1y}(\lambda)|^2 = |R_{xy}(\lambda)|^2 + |R_{x1/y}(\lambda)|^2 \left[1 - |R_{xy}(\lambda)|^2\right] \tag{8.12}$$

This function provides a measure of the linear predictability of process x based on processes N_1 and y, and can be estimated as

$$|\hat{R}_{x\cdot 1y}(\lambda)|^2 = |\hat{R}_{xy}(\lambda)|^2 + |\hat{R}_{x1/y}(\lambda)|^2 \left[1 - |\hat{R}_{xy}(\lambda)|^2\right] \tag{8.13}$$

with coherence and partial coherence estimates given by (5.5) and (8.8). Multiple coherence functions, like coherence and partial coherence functions, are bounded measures with values between 0 and 1, where zero indicates no linear relationship between the predictors and the output process.

The extension of these multivariate parameters to order greater than 1 follows from the results in Brillinger (1981) and Rosenberg *et al.* (1989). In the present report we will adopt a similar notation for vector valued and matrix valued processes. $M(t)$ represents an r-vector valued stationary interval input process, and $N(t)$ an s-vector valued stationary interval output process, where interval processes, defined by Brillinger (1972), include both point processes and time series with stationary increments. Thus the component processes, $M_1, \ldots, M_r$ and $N_1, \ldots, N_s$, may be either point processes or time series. (This notation should not be confused with the previous sections where N_0 and N_1 were used to represent individual point processes). $F_{MM}(\lambda)$ is then an $r \times r$ matrix of spectral densities whose principal diagonal consists of the auto-spectra of the components of $M(t)$, and the off-diagonal elements the cross-spectra between these components. A similar definition holds for the $s \times s$ spectral density matrix $F_{NN}(\lambda)$. These matrices are formed by direct substitution of estimates, (5.2), of the appropriate pairwise spectra at each frequency.

The elements of the matrix

$$F_{NN}(\lambda) - F_{NM}(\lambda)F_{MM}^{-1}(\lambda)F_{MN}(\lambda) \tag{8.14}$$

are defined as partial spectra between components of $N(t)$ after removing the linear contribution of $M(t)$. The -1 superscript indicates a complex valued matrix inversion operation. For $r = s = 1$, (8.14) can be seen to reduce to the same form as (8.3). Evaluation of (8.14) involves filling in the appropriate elements of each matrix and solving by standard complex matrix arithmetic at each frequency. The elements of (8.14) may be denoted as $f_{N_iN_j/M}(\lambda)$ where $i=j$ gives the partial auto-spectra, and $i \neq j$ the partial cross-spectra of the components N_i and N_j of $N(t)$ after removing the linear contribution of $M(t)$. The partial coherence between the i^{th} and j^{th} components of $N(t)$ may then be written in terms of partial spectra, following (8.4), as

$$|R_{N_iN_j/M}(\lambda)|^2 = \frac{|f_{N_iN_j/M}(\lambda)|^2}{f_{N_iN_i/M}(\lambda) f_{N_jN_j/M}(\lambda)} \tag{8.15}$$

and estimation of this follows similarly to (8.8). The partial phase can also be written in terms of the entries of (8.14) as

$$\Phi_{N_iN_j/M}(\lambda) = \arg\left\{f_{N_iN_j/M}(\lambda)\right\} \tag{8.16}$$

and estimation of this partial phase follows similarly to (8.9). Following (8.10) partial cumulant density functions can be defined in terms of the elements of (8.14) as

$$q_{N_iN_j/M}(u) = \int_{-\pi}^{\pi} f_{N_iN_j/M}(\lambda) e^{i\lambda u} d\lambda \tag{8.17}$$

with estimation following from (8.11). In (8.17) the row subscript i for $N(t)$ should not be confused with the i superscript on the complex exponential of the Fourier transform.

If only one output process is under consideration ($s = 1$), then $N(t)$ reduces to a single N-process, which may be either a point-process or a time series, and the output spectral

density matrix reduces to a single auto-spectrum, $f_{NN}(\lambda)$. For this situation a multiple coherence function, $|R_{N\cdot M}(\lambda)|^2$, can be defined as

$$|R_{N\cdot M}(\lambda)|^2 = \frac{F_{NM}(\lambda)F_{MM}^{-1}(\lambda)F_{MN}(\lambda)}{f_{NN}(\lambda)} \tag{8.18}$$

This function represents the multiple coherence at frequency λ of the N-process with the processes $M_1, \ldots, M_r$. Estimates of (8.18) provide a measure, at a given frequency λ, of the linear predictability of the N-process based on the combined r inputs. In (8.18) $F_{NM}(\lambda)$ represents a row vector with r entries which are the cross-spectra between each of the components of $M(t)$ and the N-process. Similarly, $F_{MN}(\lambda)$ represents a column vector with r entries. Estimation of multiple coherence functions can be achieved by filling in the various matrix elements in (8.18) in the same manner as for (8.14), and evaluating to provide an estimate.

We conclude this section by remarking that the first order partial parameters defined by equations (8.1) to (8.13) are valid for any combination of point process and/or time series data. This follows directly from the derivation of (8.14) to (8.18).

IX. CONFIDENCE LIMITS FOR ESTIMATES OF MULTIVARIATE PARAMETERS

The setting of confidence limits for the multivariate parameters defined in the previous section involves steps similar to those used in Section VI. The asymptotic behaviour of partial coherency estimates is the same as that of coherency estimates, and the covariance structure for partial coherence estimates is the same for all values of r, s (Brillinger, 1981; Amjad, 1989). Following this, expression (9.1) can be used to construct confidence limits for partial coherence estimates of all orders in the manner of (6.5).

$$\mathrm{var}\left\{\mathrm{Tan}h^{-1}|\hat{R}_{N_iN_j/M}(\lambda)|\right\} = \frac{1}{2L} \tag{9.1}$$

For the case of independence, $|R_{N_iN_j/M}(\lambda)|^2 = 0$, the distribution of $|\hat{R}_{N_iN_j/M}(\lambda)|^2$ can be evaluated in terms of the incomplete Beta function with parameters 1 and (L-r-1), the upper 95% confidence limit for non-zero partial coherence estimates is then given at the $100\alpha\%$ point by $1-(1-\alpha)^{1/(L-r-1)}$ where r is the number of predictors and L the number of disjoint sections (Brillinger, 1981; Amjad, 1989). An estimate of the upper 95% confidence limit is then provided by

$$1 - (0.05)^{1/(L-r-1)} \tag{9.2}$$

Values of estimated partial coherence lying below this line can be taken as evidence for the lack of a linear association between the two processes after removal of the effects of the r predictors.

Expressions for the variance of partial phase estimates can be found in Brillinger (1981) for time series data, and Amjad (1989) for point process data. Following these results we define the variance of the estimate of the partial phase (8.16) as

$$\mathrm{var}\left\{\hat{\Phi}_{N_iN_j/M}(\lambda)\right\} = \frac{1}{2L}\left(\frac{1}{|R_{N_iN_j/M}(\lambda)|^2} - 1\right) \tag{9.3}$$

where L is the number of disjoint sections. In practice an estimate of the partial coherence can be substituted into (9.3) and estimates of upper and lower 95% confidence limits constructed in the manner of (6.8).

At present it is not clear how to extend the integral procedure given in Section VI to the multivariate case. However, since (6.9) is based on the assumption of independence then, under the same assumption it can provide an estimate of the variance of partial cumulant densities. With this reservation in mind the variance of partial cumulant estimates based

on (8.17), $\text{var}\{\hat{q}_{N_iN_j/M}(u)\}$, can be estimated using (6.10), with the corresponding 95% confidence limits given by (6.11).

The variance of multiple coherence estimates has been discussed for time series data by Brillinger (1981), and for point process data by Amjad (1989). These results extend directly to estimates of hybrid multiple coherence (8.18) as set out below. To construct confidence limits for multiple coherence estimates the arctanh transformation can be applied, and the variance, $\text{var}\{\text{Tanh}^{-1}|\hat{R}_{N\cdot M}(\lambda)|\}$, can be approximated by 1/2L. A confidence interval can then be constructed in the manner of (6.5). In the case of independence, $|R_{N\cdot M}(\lambda)|^2 = 0$, the distribution of (8.18) can be approximated by a Beta distribution with parameters r and (L − r). From this a test for non-zero multiple coherence at the $100(1-\alpha)\%$ significance level can be expressed in terms of an F distribution as

$$\frac{rF_\alpha}{L + r(F_\alpha - 1)} \tag{9.4}$$

where F_α is the $100\alpha\%$ point of the F distribution with 2r and 2(L − r) degrees of freedom. This can be obtained from standard tables of the F distribution. Values of estimated multiple coherence lying below this line can be taken as evidence for the lack of a linear association between the inputs, $M(t)$, and the output N-process at a given frequency λ.

X. EXAMPLES OF MULTIVARIATE PARAMETERS

The multivariate parameters defined in Section VIII will be used to investigate further the dependencies between the four signals. As in Section VII, all parameters in this section have been estimated using T = 1024. Turning first to the relationship between the single motor units and the tremor, application of the multiple coherence estimate, (8.18), will provide a measure of the linear dependence of the tremor upon the combined activity of both motor units. An estimate of this, $|\hat{R}_{x\cdot 10}(\lambda)|^2$, is shown in Fig. 9. Included in the graph is an estimate of the upper 95% confidence limit based on the hypotheses of independence, constructed from (9.4) where L = 175, r = 2 and (from standard tables) $F_{4,346;0.05} = 2.40$, giving a value of 0.027 which is shown as the dashed horizontal line in Fig. 9. This estimate exhibits the same peaks around 5 and 26 Hz as the ordinary coherence estimates in Fig. 4b, c, but with an increase in magnitude. For independent predictors, the multiple coherence is approximately equal to the sum of the individual coherences (This can be proved by setting the off-diagonal elements in the spectral matrix of $M(t)$ to zero in (8.18)). The multiple coherence estimate shown in Fig. 9 is less than the sum of the two estimates in Fig. 4b, c. This indicates correlated predictors, as in fact illustrated by Fig. 4a. The peak coherence is now around 0.4 in the 5 Hz and 20–30 Hz bands, with a maximum value and 95% confidence limits of 0.409 ± 0.079 at 26.4 Hz. This indicates that the two observed motor unit discharges can predict around 40% of the variability in the tremor signal at these frequencies. This level of predictability from only two motor units suggests motor unit coupling at these frequencies throughout the population of active motor units. The maximum is close to the peak magnitude of the surface EMG–tremor coherence, $|\hat{R}_{xy}(\lambda)|^2$, in the 20–30 Hz band (Fig. 7d), providing further evidence that the 20–30 Hz band of motor unit coupling is well represented in the surface EMG, whereas the 5 Hz band is poorly represented. Partial parameters provide the appropriate tools for further investigation of this observation.

Figure 10a shows an estimate of the first order partial coherence, (8.15), between motor unit 0 and motor unit 1 using the surface EMG as the predictor, $|\hat{R}_{10/y}(\lambda)|^2$, along with an estimate of the upper 95% confidence limit based on the assumption of independence, given by (9.2). For L = 175 and r = 1 this has the value 0.0172, and is shown as the dashed line in Fig. 10a. The corresponding partial cumulant density estimate, $\hat{q}_{10/y}(u)$, is shown in Fig. 10b, along with the expected value (dashed line) and the upper and lower 95% confidence limits based on the assumption of independence. Comparison with the ordinary coherence between the two motor units illustrated in Fig. 4a shows that the motor unit coupling between 20–30 Hz can be entirely predicted using the surface EMG signal. In

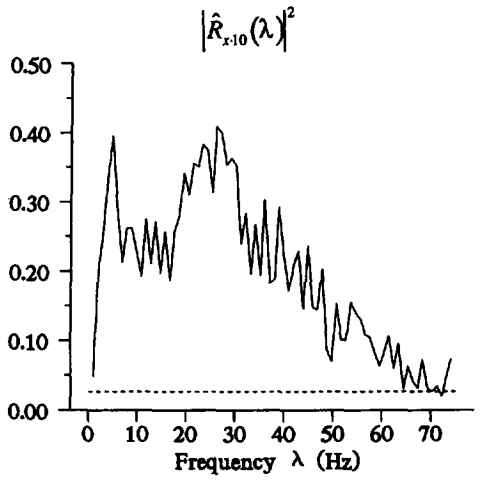

Fig. 9. Estimated multiple coherence between both motor units and the tremor $|\hat{R}_{x\cdot 10}(\lambda)|^2$. The horizontal dashed line represents an estimate of the upper 95% confidence limit based on the assumption of independence.

contrast the coupling around 5 Hz remains almost unchanged in the partial coherence. This reduction in the partial coherence is matched by a corresponding reduction in the height of the central peak and side bands in the partial cumulant in Fig. 10b compared with the same features in Fig. 8a.

It was noted in Section VII that the coupling between a motor unit and the tremor signal involved the same frequency bands as the motor unit–motor unit coupling. It can be hypothesized that this reflects a process whereby the frequency content of the mechanism which is responsible for the motor unit coupling is transmitted as a force or muscle length signal to the tremor. If this were the case, and the processes involved are linear, then the motor unit coupling in these frequency bands can be predicted from the tremor signal. This hypothesis, that motor unit coupling can be predicted by the tremor signal, can be tested by examining the partial coherence, $|\hat{R}_{10/x}(\lambda)|^2$, and cumulant, $\hat{q}_{10/x}(u)$, estimates between the motor unit pair using the tremor signal as the predictor. These estimates are shown in Fig. 10c, d, respectively, with estimated confidence limits (which are the same as Figs. 10a, b, respectively). Apart from some residual coupling below 5 Hz, the partial coherence shows an almost complete absence of any relationship in this case, which indicates that the above hypothesis is largely true. In the time domain the residual coupling results in short-term synchrony with a much reduced central peak in the cumulant, Fig. 10d. The central peak in the original cumulant estimate, $\hat{q}_{10}(u)$ (Fig. 8a), is therefore the consequence of several processes, one of which is motor unit coupling in the 20–30 Hz range. Fig. 10 also shows that the tremor signal provides a better predictor of motor unit coupling than the surface EMG signal.

In Fig. 11 are shown second order partial coherence, $|\hat{R}_{10/xy}(\lambda)|^2$, and second order partial cumulant density, $\hat{q}_{10/xy}(u)$, estimates (based on 8.15 and 8.17) using both the tremor signal and the surface EMG as predictors. These estimates show a slight reduction in the magnitude of the significant features in Fig. 10, and illustrate that the frequency content of the linear motor unit coupling in this case is almost entirely contained in the surface EMG and finger acceleration signals. The residual coupling, which occurs below 5 Hz, can be interpreted in two ways. It may be due to some other linear coupling between the two motor unit discharges, or it may reflect a non-linear component in the coupling which cannot be predicted by the linear multivariate parameters.

XI. LINEAR BIVARIATE AND MULTIVARIATE SYSTEM ANALYSIS

The previous analyses have made no assumption about causality of the observed signals,

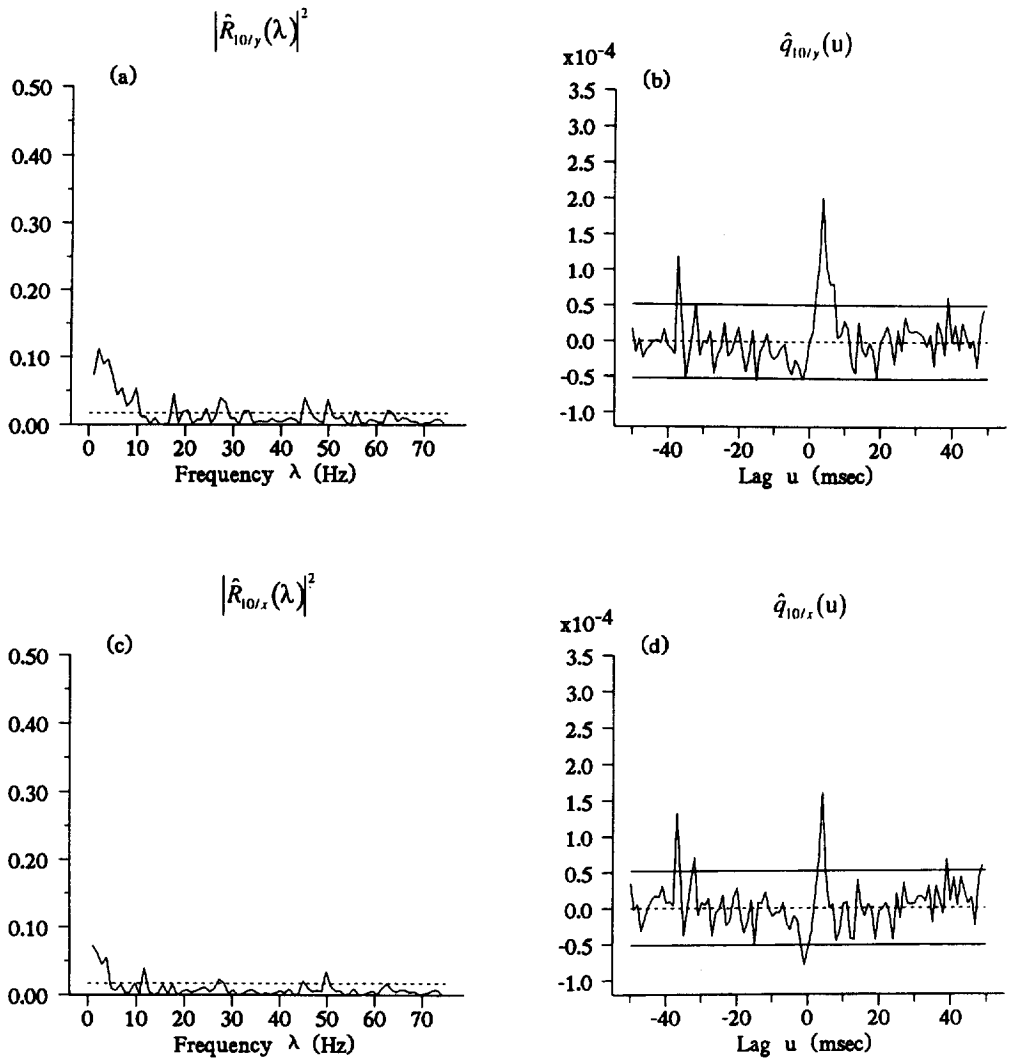

Fig. 10. (a) Estimated first order partial coherence between motor unit 0 and motor unit 1, using the surface EMG as predictor, $|\hat{R}_{10/y}(\lambda)|^2$, and (b) corresponding first order partial cumulant density estimate $\hat{q}_{10/y}(u)$. (c) Estimated first order partial coherence between motor unit 0 and motor unit 1, using the tremor as predictor, $|\hat{R}_{10/x}(\lambda)|^2$, and (d) corresponding first order partial cumulant density estimate, $\hat{q}_{10/x}(u)$. The horizontal dashed lines in (a) and (c) represent an estimate of the upper 95% confidence limit based on the assumption of independence. The horizontal lines in (b) and (d) show the asymptotic value (dashed line at zero) and estimated upper and lower 95% confidence limits based on the assumption of independence.

the situation referred to by Jenkins and Watts (1968) as signals which arise "on an equal footing". An example of this for the present data is the two motor units, N_0 and N_1. In many cases however, the signals being studied are causally related, where one signal can be regarded as the input and the other signal as the output of a linear system.

Examples of this for the present data are the three {input, output} pairs: $\{N_0, x\}$, $\{N_1, x\}$ and $\{y, x\}$. In this situation, the theory of linear systems can be brought to bear on the analysis. The assumptions underlying the analysis in this section are that the system under study is linear and time invariant. The theory of general multivariate linear time series systems is given by Jenkins and Watts (1968) and Brillinger (1981), the analogous theory for multivariate point-process systems by Amjad (1989). Single input–single output hybrid systems are discussed in Rosenberg *et al.* (1982) and Rigas (1983).

For input point process N_1 and output time series x the transfer function, $A_{x1}(\lambda)$, is defined as (Rigas, 1983)

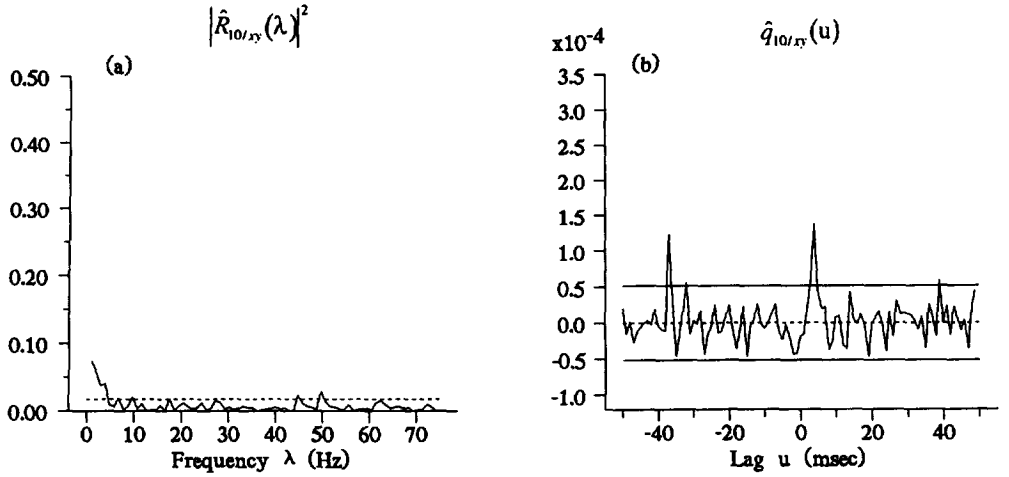

Fig. 11. (a) Estimated second order partial coherence between motor unit 0 and motor unit 1, using the tremor and surface EMG as predictors, $|\hat{R}_{10/xy}(\lambda)|^2$. The horizontal dashed line represents an estimate of the upper 95% confidence limit based on the assumption of independence. (b) Corresponding second order partial cumulant density estimate, $\hat{q}_{10/xy}(u)$. The horizontal lines show the asymptotic value (dashed line at zero) and estimated upper and lower 95% confidence limits based on the assumption of independence.

$$A_{x1}(\lambda) = \frac{f_{x1}(\lambda)}{f_{11}(\lambda)} \tag{11.1}$$

which can be estimated as

$$\hat{A}_{x1}(\lambda) = \frac{\hat{f}_{x1}(\lambda)}{\hat{f}_{11}(\lambda)} \tag{11.2}$$

The transfer function is a complex valued function, and it is customary to consider gain and phase functions separately. The gain, $G_{x1}(\lambda)$, is the magnitude of the transfer function, and may be estimated by

$$\hat{G}_{x1}(\lambda) = |\hat{A}_{x1}(\lambda)| = \frac{|\hat{f}_{x1}(\lambda)|}{\hat{f}_{11}(\lambda)} \tag{11.3}$$

Since the denominator in (11.1) is a positive real valued function the phase of $A_{x1}(\lambda)$ is the same as the phase of the cross-spectrum, $\Phi_{x1}(\lambda)$, defined in (5.6), and can be estimated from (5.7).

The time domain equivalent of the transfer function, denoted by $a_{x1}(u)$, is defined as the inverse Fourier transform of $A_{x1}(\lambda)$ as (Rigas, 1983)

$$a_{x1}(u) = \frac{1}{2\pi}\int_{-\pi}^{\pi} A_{x1}(\lambda)e^{i\lambda u}d\lambda \tag{11.4}$$

which can be estimated as

$$\hat{a}_{x1}(u) = \frac{1}{T}\sum_{|j|\leq T/2} \hat{A}_{x1}(\lambda_j)e^{i\lambda_j u} \tag{11.5}$$

where $\lambda_j = 2\pi j/T$. The function $a_{x1}(u)$ is the average impulse response function of the linear system with input N_1 and output x. The above expressions are valid for any combination of time series and/or point process linear systems analysis.

Extension of the above parameters to the multivariate case follows from the multivariate parameters defined in Section VIII. In the general case we are dealing with a system which has r inputs represented by the r-vector valued stationary interval process, $\boldsymbol{M}(t)$, and s outputs represented by the s-vector valued stationary interval process, $\boldsymbol{N}(t)$, as

defined in Section VIII. In this case the transfer function, $A_{NM}(\lambda)$, and impulse response function, $a_{NM}(u)$, are complex and real valued r × s matrix functions respectively. The elements $A_{N_iM_j}(\lambda)$ and $a_{N_iM_j}(u)$ are the transfer function and impulse response function of the i^{th} output with respect to the j^{th} input, respectively. These can be defined and estimated using the above equations. When r = s = 1 the system under study reduces to single input–single output.

It is also possible to define and estimate partial transfer functions and partial impulse response functions. Thus, if we denote as M' the (r − 1) components of $M(t)$ omitting M_j then the partial transfer function between M_j and N_i after removal of the common linear effects of M' is defined as

$$A_{N_iM_j/M'}(\lambda) = \frac{f_{N_iM_j/M'}(\lambda)}{f_{M_jM_j/M'}(\lambda)} \tag{11.6}$$

This is the ratio of the partial cross-spectrum of order (r − 1) to the partial auto-spectrum of order (r − 1), and can be estimated by direct substitution of the appropriate partial spectra in the manner of (11.2). From (11.6) can be derived the partial gain of order (r − 1), $G_{N_iM_j/M'}(\lambda)$, and partial impulse response of order (r − 1), $a_{N_iM_j/M'}(u)$ the definition and estimation of these quantities follows directly from the above single input–single output case. Also associated with $A_{N_iM_j/M'}(\lambda)$ is the partial phase of order (r − 1), $\Phi_{N_iM_j/M'}(\lambda)$, see Section VIII.

In situations where causality is known, or can be inferred, between two or more processes, application of the techniques defined in this section can extend the range of questions that can be investigated. In particular the two related problems of predicting the output of a (linear) system given the input signal and determining the characteristics of the (linear) system which converts the input signal to the output signal can be addressed. The first problem is discussed in Jenkins and Watts (1968) for time series systems, and the latter problem in Brillinger (1983), also for time series systems, where it is considered in the context of the determination of an optimum linear filter. Point process system identification techniques are discussed in Brillinger (1975b), Brillinger *et al.* (1976), Rosenberg *et al.* (1982) and Halliday *et al.* (1992).

In terms of regression analysis, the transfer function represents complex regression coefficients at each frequency, where the gain and phase give the amplitude and phase by which the input series should be altered to obtain an optimum fit to the output series. The goodness of fit is measured by the appropriate coherence or partial coherence estimate.

XII. CONFIDENCE LIMITS FOR LINEAR SYSTEM TRANSFER FUNCTION PARAMETER ESTIMATES

Confidence limits for the parameters in the previous section can be set using methods similar to those used in Sections VI and IX. For multivariate time series systems confidence limits for parameter estimates are discussed in Brillinger (1981), analogous results for point process systems analysis are developed in Amjad (1989). The single input–single output hybrid case is discussed in Rigas (1983). It is customary to plot gain functions on a log scale. The variance of the natural log of the hybrid gain estimate is (Rigas, 1983)

$$\operatorname{var}\{\ln(\hat{G}_{x1}(\lambda))\} = \frac{1}{2L}\left(\frac{1}{|R_{x1}(\lambda)|^2} - 1\right) \tag{12.1}$$

The variance can be seen to be the same as that of the estimated phase, (6.7). In practice an estimate of the coherence function can be substituted into (12.1), and using a base 10 logarithmic transform, an upper and lower 95% confidence interval about the estimated gain can be set as

$$\log_{10}(\hat{G}_{x1}(\lambda)) \pm 1.96\left[\frac{(\log_{10}(e))^2}{2L}\left(\frac{1}{|\hat{R}_{x1}(\lambda)|^2}-1\right)\right]^{1/2} \tag{12.2}$$

The variance of impulse response functions has been calculated in Rigas (1983), under the assumption of input/output independence, using a similar integral procedure to that for cumulant density functions. The variance of the estimated impulse response function, (11.5), can then be approximated by

$$\text{var}\{\hat{a}_{x1}(u)\} \approx \frac{1}{2\pi R}\int_{-\pi}^{\pi} f_{xx}(\lambda)/f_{11}(\lambda)d\lambda \tag{12.3}$$

where R is the record length, and $f_{xx}(\lambda)$ and $f_{11}(\lambda)$ are the auto-spectra of the component processes. In practice this expression can be estimated using a discrete summation, and substitution of auto-spectra based on (5.2) into equation (12.3). The appropriate expression to estimate the variance is then

$$\text{var}\{\hat{a}_{x1}(u)\} \approx \left(\frac{1}{R}\right)\left(\frac{1}{T}\right)\sum_{j=1}^{T/2-1} 2\hat{f}_{xx}(\lambda_j)/\hat{f}_{11}(\lambda_j) \tag{12.4}$$

where $\lambda_j = 2\pi j/T$, R is the record length, and T is the segment length used in the estimation of the finite Fourier transforms (4.1) and (4.2). This expression is based on the assumption of two independent processes. In this case the asymptotic value and upper and lower 95% confidence interval for the estimated impulse response function (11.5) are given by

$$0 \pm 1.96\left[\left(\frac{1}{R}\right)\left(\frac{1}{T}\right)\sum_{j=1}^{T/2-1} 2\hat{f}_{xx}(\lambda_j)/\hat{f}_{11}(\lambda_j)\right]^{1/2} \tag{12.5}$$

Expressions (12.3) to (12.5) are valid for other combinations of time series and/or point process linear systems impulse response functions by substitution of the appropriate spectra.

The extension to multivariate systems follows from the results presented in Brillinger (1981) and Amjad (1989). For partial gain estimates $\hat{G}_{N_iM_j/M'}(\lambda)$ we have

$$\text{var}\left\{\ln\left(\hat{G}_{N_iM_j/M'}(\lambda)\right)\right\} = \frac{1}{2L}\left(\frac{1}{|R_{N_iM_j/M'}(\lambda)|^2}-1\right) \tag{12.6}$$

and a confidence limit can be derived in the manner of (12.2).

At present it is not clear how to extend the integral procedure expression given in (12.3) to the multivariate case. However, since this procedure is based on the assumption of independence, then under the same assumption it can provide an estimate of the variance of partial impulse response functions. With this reservation in mind the variance of partial cumulant estimates based on (11.5) and (11.6), $\text{var}\left\{\hat{a}_{N_iN_j/M'}(u)\right\}$, can be estimated using (12.4), with the corresponding 95% confidence limits following from (12.5).

XIII. EXAMPLES OF LINEAR SYSTEM TRANSFER FUNCTION PARAMETERS

As examples of single input–single output linear systems we will consider the three input–output pairs $\{N_0, x\}$, $\{N_1, x\}$ and $\{y, x\}$. Estimates of the three gain functions, $\hat{G}_{x0}(\lambda)$, $\hat{G}_{x1}(\lambda)$ and $\hat{G}_{xy}(\lambda)$, are shown in Fig. 12. These estimates are plotted on a $\log_{10}$ scale and include the estimated upper and lower 95% confidence limits for each estimate. A useful model for the interpretation of these gain estimates is the log gain plot of a resonant system (Jenkins and Watts, 1968, Ch. 2). This has a constant gain at low frequencies which rises to a peak at the resonant frequency before tailing off. The two motor unit–tremor gain estimates have similar envelopes with small peaks at about 5, 20 and 28 Hz (Fig. 12a, c). The confidence limits around these frequencies indicate that these peaks are significant, implying a resonant system with multiple periodicities. The gain estimate for the EMG–

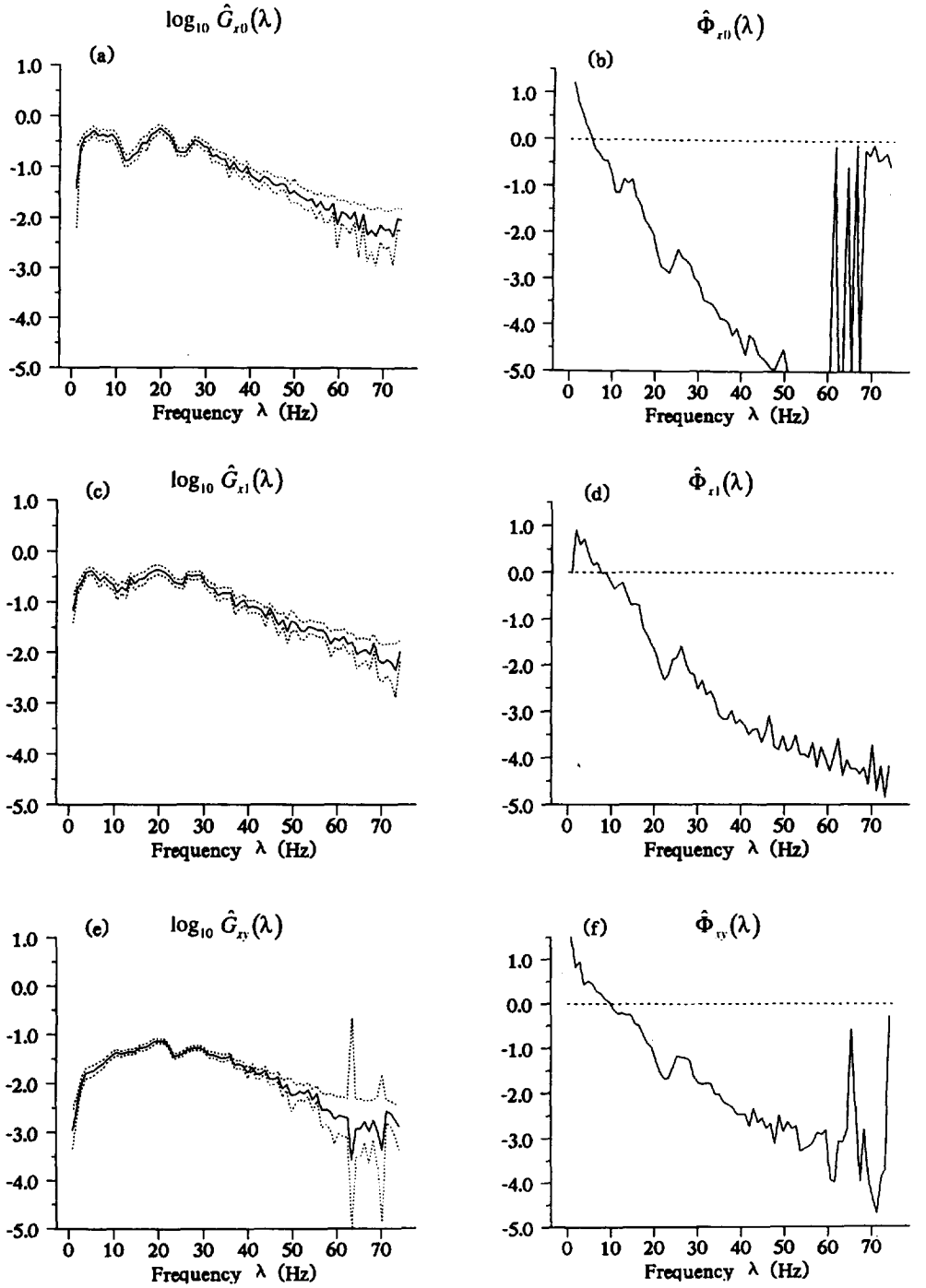

Fig. 12. Log plots of estimated gain between (a) motor unit 0 and tremor, $\hat{G}_{x0}(\lambda)$, (c) motor unit 1 and tremor, $\hat{G}_{x1}(\lambda)$, and, (e) surface EMG and tremor, $\hat{G}_{xy}(\lambda)$. The dotted lines in (a) (c) and (e) represent upper and lower 95% confidence limits for each estimate at each frequency. Estimated phase between (b) motor unit 0 and tremor, $\hat{\Phi}_{x0}(\lambda)$, (d) motor unit 1 and tremor, $\hat{\Phi}_{x1}(\lambda)$, and, (f) surface EMG and tremor, $\hat{\Phi}_{xy}(\lambda)$. Phase estimates are plotted in unconstrained form.

tremor system (Fig. 12e) has a similar envelope, with a maximum at 20 Hz, but with no clear peak around 5 Hz and a gain curve which drops off more rapidly at low frequencies.

The corresponding phase plots are those in Fig. 12b, d and f, respectively, reproduced from Fig. 6. It was seen in Section VII that a pure time delay model was insufficient to describe these phase curves over the range of significant coherence estimates in Fig. 4. The

gain plots in Fig. 12 suggest a system with multiple resonances, an accurate model of these including the biomechanics of muscle, tendon, joint and limb is likely to result in a transfer function description of order greater than two which will have a non-constant phase curve. A second factor which may explain the phase lead at low frequencies is the use of an accelerometer to measure tremor. Acceleration represents a double differentiation of displacement, the output of a differentiation circuit has a phase lead with respect to the input (e.g., see Jenkins and Watts, 1968). A simulation study would provide the means to test these hypotheses, as well as a guide to interpretation of gain and phase estimates.

The output signal in the three transfer functions is the same, the tremor signal x, thus we see that the transfer function has more resonant peaks in response to individual motor unit activity than for surface EMG activity. This is also clear from the estimated impulse response functions, shown in Fig. 13. The two motor unit–tremor impulse response estimates have more complex time-courses, perhaps indicating interactions between several oscillatory components. When compared with the corresponding hybrid cumulant density estimates in Fig. 8 there is a reduction in the oscillations prior to time zero, and is particularly obvious for the motor unit 0–tremor relation. From this it can be concluded that the oscillation prior to time zero in the cumulant density estimates reflect periodicities in the input signals which are not present in the transfer function estimates. These oscillations will also map onto positive lag values, therefore the time-course of these three impulse response functions can be expected to provide a more accurate representation of the acceleration response to motor unit and EMG activity. The impulse response estimates for the two motor units (Fig. 13a, b) both exhibit a clear peak prior to time zero. This appears to indicate that the response occurs before the stimulus, and represents a situation where the linear transfer function model, (11.1) and (11.4), does not provide a complete description of the input output relationship. In a study of synaptic interactions between *Aplysia* neurons, Brillinger *et al.* (1976) attributed features prior to time zero in estimated impulse response functions as an indication of a non-linear interaction. A similar interpretation placed on the estimates in Fig. 13 indicates that a move to a non-linear model may be appropriate in the present case.

We conclude the linear analysis with the second order partial parameter estimates shown in Fig. 14. The four graphs show estimates of the second order partial coherence between surface EMG and tremor with motor unit 0 and motor unit 1 as predictors, $|\hat{R}_{xy/10}(\lambda)|^2$, Fig. 14a, along with the corresponding partial cumulant density, $\hat{q}_{xy/10}(u)$, Fig. 14b, partial gain, $\hat{G}_{xy/10}(\lambda)$, Fig. 14c, and partial impulse response, $\hat{a}_{xy/10}(u)$, Fig. 14d. These parameters investigate to what extent the surface EMG to tremor correlation can be predicted from a pair of correlated motor units. The partial coherence and partial gain estimates (Fig. 14a, c), show a reduction in magnitude over a broad range of frequencies when compared with the normal coherence (Fig. 4d) and gain (Fig. 12c). The time-course of the partial cumulant and partial impulse response estimates (Fig. 14b, d) are little changed from the normal cumulant (Fig. 8d) and impulse response estimates (Fig. 13c). Thus, while it is possible to predict to a large extent the motor unit coupling from the surface EMG and tremor signals (Figs. 10a, c, 11a), the reverse is not true. This suggests that the tremor and surface EMG are richer signals than the two motor unit discharges.

XIV. HIGHER ORDER PARAMETERS

In this section we will introduce higher order hybrid parameters, which will be used to investigate one specific question, namely, the contribution from correlated motor unit discharges to physiological tremor that results purely from the correlation. The extension to the hybrid case of previous results on higher order time series and higher order point process analyses is more complicated than for the linear spectral based measures. In the third order case a major difference between time series and point process parameters is the non-equivalence of third order moment functions and third order cumulant density functions. For time series, the third order moment and third order time series cumulant density functions are equivalent (see e.g., Mendel, 1991). In the point process case the

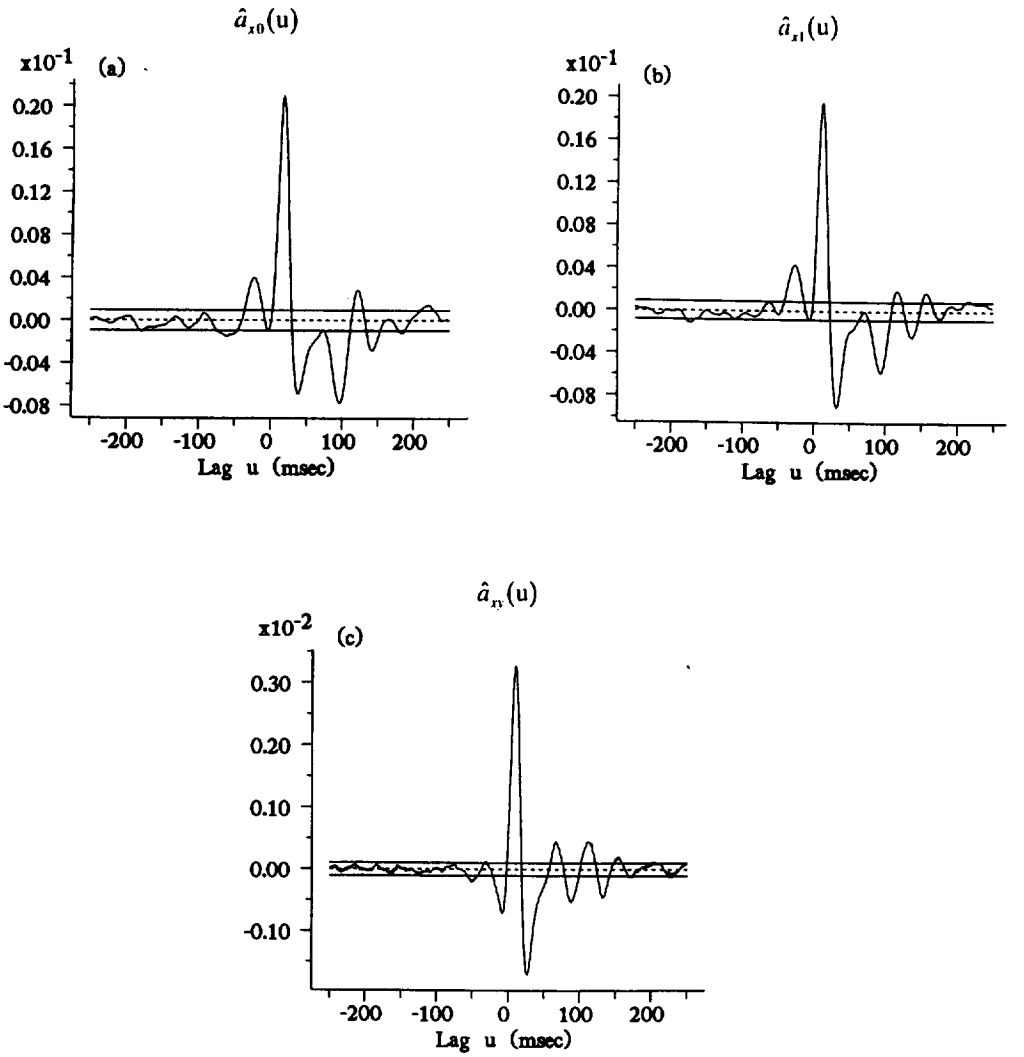

Fig. 13. Estimated impulse response between (a) motor unit 0 and tremor, $\hat{a}_{x0}(u)$, (b) motor unit 1 and tremor, $\hat{a}_{x1}(u)$, and, (c) surface EMG and tremor, $\hat{a}_{xy}(u)$. The horizontal lines in each graph show the asymptotic value (dashed line at zero) and estimated upper and lower 95% confidence limits based on the assumption of independence.

analogous functions to moment functions are product density functions, and third order point process cumulant densities and third order product densities are not equivalent (Conway *et al.*, 1993). Higher order analyses of point process data have been discussed in Brillinger (1975b), Amjad *et al.* (1989) and Conway *et al.* (1993). References to higher order analyses of time series include Brillinger (1965), Rosenblatt (1983), Nikias and Raghuveer (1987) and Mendel (1991).

The specific problem to be addressed is the contribution from correlated motor unit discharges to physiological tremor which can be attributed to the correlation. This contribution must be assessed separately from the contribution which each individual motor unit makes to the tremor. Thus we are interested in the joint statistical dependence between three random processes, which requires the use of a third order measure. The appropriate measure is the third order hybrid cumulant density function (Amjad *et al.*, 1994a). We start with the direct definition and estimation of this cumulant density in the time domain. Following standard convention (Rosenblatt, 1983) this third order cumulant can be derived from the expression

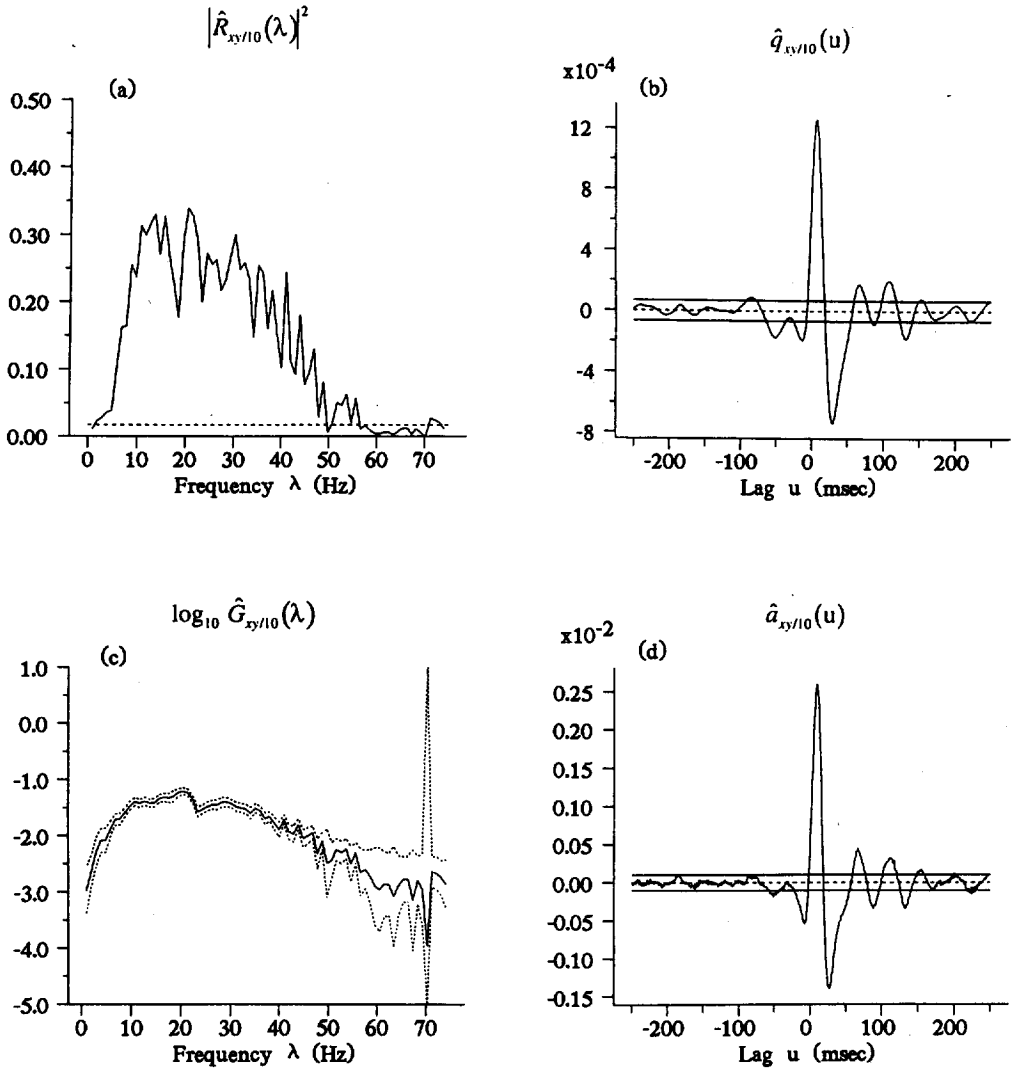

Fig. 14. Estimates of second order partial parameters between surface EMG and tremor with motor unit 0 and motor unit 1 as predictors. (a) Estimated partial coherence, $|\hat{R}_{xy/10}(\lambda)|^2$, horizontal dashed line represents an estimate of the upper 95% confidence limit based on the assumption of independence. (b) Corresponding partial cumulant density estimate, $\hat{q}_{xy/10}(u)$. (c) Log plot of estimated gain, $\hat{G}_{xy/10}(\lambda)$, the dotted lines represent upper and lower 95% confidence limits for the estimate at each frequency. (d) Estimated partial impulse response, $\hat{a}_{xy/10}(u)$. The horizontal lines in (b) and (d) show the asymptotic value (dashed line at zero) and estimated upper and lower 95% confidence limits based on the assumption of independence.

$$\begin{aligned}\text{cum}\{x(t+u), dN_1(t+v), dN_0(t)\} &= q_{x10}(u,v)\,dv\,dt \\ &= E\{x(t+u)(dN_1(t+v) - P_1 dv)\,(dN_0(t) - P_0 dt)\}\end{aligned} \tag{14.1}$$

where x is a zero mean time series, N_0 and N_1 are two point processes, and $dN_0(\cdot)$ and $dN_1(\cdot)$ are the differential increments of these point processes. P_0 and P_1 are the mean intensities of processes N_0 and N_1 respectively, as defined in Section VI. The two terms $(dN_1(t+v) - P_1 dv)$ and $(dN_0(t) - P_0 dt)$ are zero mean differential increments of N_1 and N_0 respectively. Expansion of (14.1) leads to the definition of the third order hybrid cumulant density function between N_0, N_1 and x, $q_{x10}(u,v)$, at lags u and v as

$$q_{x10}(u,v) = P_{x10}(u,v) - P_{x1}(u-v)P_0 - P_{x0}(u)P_1 \tag{14.2}$$

Taking the individual terms on the right hand side of (14.2), $P_{x10}(u,v)$ may be viewed as a hybrid product moment which provides a measure of the contribution from a spike in process N_0 and a spike in process N_1 to the tremor signal. The timing convention for this function is the same as for $q_{x10}(u,v)$, namely a reference time t, corresponding to an N_0 spike, with an N_1 spike at time $(t+v)$ and a tremor sample at time $(t+u)$. The term $P_{x10}(u,v)$ represents the contribution from both spikes in the pair to the tremor and necessarily contains the individual contribution from each spike. These individual contributions are subtracted out by the last two terms in the RHS of (14.2), the first term, $P_{x1}(u-v)P_0$, refers to the contribution from the N_1 spike $(u-v)$ time units prior to the tremor sample, and the second term refers to the contribution from the N_0 spike u time units prior to the tremor sample. These two terms have the form of spike triggered averages which are scaled by the mean intensities of the other spike trains, P_0 and P_1. The functions $P_{x0}(\cdot)$ and $P_{x1}(\cdot)$ can also be called second order hybrid product moments in line with the description of $P_{x10}(u,v)$. In the case of a zero mean time series, x, the spike triggered average $P_{x0}(u)$ is equivalent to the hybrid cumulant $q_{x0}(u)$, (5.8) (Rosenberg *et al.*, 1982; Rigas, 1983).

The indirect definition of the third order hybrid cumulant density via the frequency domain is given (cf. 5.8) by

$$q_{x10}(u,v) = \int_{-\pi}^{\pi}\int_{-\pi}^{\pi} f_{x10}(\lambda,\mu)e^{i(\lambda u+\mu v)}d\lambda\, d\mu \tag{14.3}$$

where $f_{x10}(\lambda, \mu)$ is the third order hybrid cross bi-spectrum.

The estimation of (14.2) involves construction of estimates of the individual terms in the equation. The mean intensity of P_1 can be estimated by

$$\hat{P}_1 = \frac{N_1(R)}{R} \tag{14.4}$$

where R is the record length. A similar definition holds for estimation of P_0. The second order hybrid product moment functions can be estimated as

$$\hat{P}_{x1}(u-v) = \frac{1}{R}\sum_{i=1}^{N_1(R)} x(t_i+u-v) \tag{14.5}$$

and

$$\hat{P}_{x0}(u) = \frac{1}{R}\sum_{j=1}^{N_0(R)} x(\sigma_j+u) \tag{14.6}$$

where t_i give the times of the spikes in process N_1, $(i = 1, \ldots, N_1(R))$, and σ_j give the times of the spikes in process N_0, $(j = 1, \ldots, N_0(R))$. The third order hybrid product moment can be estimated by

$$\hat{P}_{x10}(u,v) = \frac{1}{R}\sum_{j=1}^{N_0(R)} x(\sigma_j+u)|v = t_i - \sigma_j;\ i = 1,\ldots,N_1(R) \tag{14.7}$$

The final estimate of $q_{x10}(u,v)$ is constructed by direct substitution of the above estimates into (14.2). The comments about interpretation of cumulants in Section V are applicable also to third order cumulants. The value of the above cumulant density if one of the three processes x, N_1 and N_0, is independent of the other two is zero. The hybrid cumulant may assume both positive and negative values.

In other situations involving different combinations of point-process and time series data, it may be appropriate to use a different third order cumulant density function, these can be defined and estimation procedures developed using the above methods.

In the frequency domain the higher order relationship between the three processes can be examined through the use of higher order spectra. The direct estimation in the frequency domain of third order spectra follows from (5.1) and (5.2) by consideration of the product of triplets of finite Fourier transforms. For example, we can define the third order spectrum $f_{01x}(\lambda,\mu)$, suppressing dependency on section number, as (Brillinger, 1972)

$$f_{01x}(\lambda,\mu) = \lim_{T\to\infty} \frac{1}{(2\pi)^2 T} E\left\{ d^T_{N_0}(\lambda) d^T_{N_1}(\mu) \overline{d^T_x(\lambda+\mu)} \right\} \tag{14.8}$$

which can be estimated using the method of disjoint sections outlined in Section V by

$$\hat{f}_{01x}(\lambda,\mu) = \frac{1}{(2\pi)^2 LT} \sum_{l=1}^{L} d^T_{N_0}(\lambda,l) d^T_{N_1}(\mu,l) \overline{d^T_x(\lambda+\mu,l)} \tag{14.9}$$

with the finite Fourier transforms of N_0, N_1 and x defined by (4.2) and (4.1). The ordering of the processes is different from the cumulant above, this third order spectrum provides an estimate of the dependency between components at frequency λ in process N_0, and components at frequency μ in process N_1, with components at frequency $(\lambda+\mu)$ in process x. Other third order bi-spectra can be defined and estimated in a similar manner (Brillinger, 1972).

Various coefficients of bi-spectral estimates have been proposed to investigate higher order interactions in relation to particular models of how different frequency components interact (Brillinger, 1965; Godfrey, 1965; Brillinger and Rosenblatt, 1967; Subba Rao and Gabr, 1984). One non-linear model which can be investigated using bi-spectral coefficients is the frequency beating model. This model investigates to what extent components in one process can be accounted for by the product of components at different frequencies in the other two processes, resulting in frequencies which add or "beat" together. This would occur, for example, in a non-linear system where input signals are multiplied together. The coefficient defined in (14.10) can be used to provide a measure of the relative appropriateness of the frequency beating model, (Brillinger, 1965).

$$B_{01x}(\lambda,\mu) = \frac{|f_{01x}(\lambda,\mu)|^2}{f_{00}(\lambda) f_{11}(\mu) f_{xx}(\lambda+\mu)} \tag{14.10}$$

This coefficient can be estimated by direct substitution of the appropriate second and third order spectral estimates into (14.10). It is the modulus squared of the standardized third order bi-spectrum (Brillinger and Rosenblatt, 1967). Standardized bi-spectra have the advantage that they should not contain features which are due to power in the second order spectra (Godfrey, 1965). For the present data set significant estimates of $B_{01x}(\lambda, \mu)$ at a particular (λ, μ) may indicate the presence of a non-linear interaction between components of process N_0 at frequency λ, with components of process N_1 at frequency μ and components of process x at frequency $(\lambda+\mu)$. The coefficient (14.10), $B_{01x}(\lambda, \mu)$, has been called bi-coherence by some authors, although this term has also been used for other bi-spectral coefficients.

XV. CONFIDENCE LIMITS FOR ESTIMATES OF HIGHER ORDER PARAMETERS

Using the same integral procedures as described previously, (Rigas, 1983) the variance of estimates of the third order hybrid cumulant, $q_{x10}(u,v)$, based on (14.2) and under the assumption of three independent processes is given by (Amjad *et al.*, 1994a).

$$\mathrm{var}\{\hat{q}_{x10}(u,v)\} \approx \frac{2\pi}{R} \int\int f_{xx}(\lambda) f_{11}(\mu) \overline{f_{00}(\lambda+\mu)} d\lambda d\mu \tag{15.1}$$

where R is the record length, and $f_{xx}(\lambda)$, $f_{11}(\mu)$ and $f_{00}(\lambda+\mu)$ are the auto-spectra of the component processes. (15.1) can be estimated by substitution of auto-spectral estimates based on (5.2) into the above equation giving

$$\text{var}\{\hat{q}_{x10}(u, v)\} \approx \left(\frac{2\pi}{R}\right)\left(\frac{2\pi}{T}\right)^2 \sum_{i=1}^{T-1}\sum_{j=1}^{T-1} \hat{f}_{xx}(\lambda_i)\hat{f}_{11}(\lambda_j)\hat{f}_{00}(\lambda_k) \tag{15.2}$$

where $\lambda_i = 2\pi i/T$, $\lambda_j = 2\pi j/T$, $\lambda_k = 2\pi k/T$, ($k = i+j$, mod T), R is the record length, and T the segment length. The asymptotic value and upper and lower confidence limits can now be constructed in the manner of (6.11).

The variance of the estimated third order hybrid bi-spectrum (14.9) following (Brillinger and Rosenblatt, 1967) is

$$\text{var}\{\hat{f}_{01x}(\lambda, \mu)\} \approx \frac{2\pi}{(B_T)^2 R} f_{00}(\lambda) f_{11}(\mu)\overline{f_{xx}(\lambda+\mu)} \tag{15.3}$$

where B_T is the spectral band-width, and R the record length. For the estimate (14.9) the spectral band-width can be estimated by ($2\pi/T$). Expression (15.3) contains values of the second order spectra at different frequencies. The distribution of the coefficient $B_{01x}(\lambda, \mu)$, (14.10), has been considered by Huber *et al.* (1971). In the case of a true population bi-spectrum value of zero, the distribution is exponential with a mean value of

$$\frac{T}{2\pi L} \tag{15.4}$$

We can therefore set an upper 95% confidence limit at (3 T/2π L), and estimated values of (14.10) which exceed this level may indicate the presence of non-linear interactions at approximately the 5% level of significance.

XVI. EXAMPLES OF THIRD ORDER ANALYSIS

Figure 15 shows an estimate of the third order hybrid cumulant density function between x, N_0 and N_1, $q_{x10}(u, v)$, plotted for values of u from 0 to 200 msec, and v from 0 to 20 msec. There is significant structure in this estimate concentrated along a line corresponding to fixed spacing between motor unit events (constant v). The time-course of this effect is plotted in Fig. 16a, corresponding to $\hat{q}_{x10}(u, 4)$ for u = 0 to 250 msec, the fixed value of v = 4 msec represents the maximum in the surface plot of Fig. 15. This section includes an estimate of the expected value and upper and lower 95% confidence limits based on the assumption of three independent processes, estimated from (15.2). For comparative purposes the two second order hybrid cumulant density estimates $\hat{q}_{x0}(u)$ and $\hat{q}_{x1}(u)$ (from Fig. 8b, c) are re-plotted in Fig. 16b, c, over the range u = 0 to 250 msec. From examination of Figs. 15 and 16 we can conclude that there is a significant third order contribution from the two motor unit discharges to the tremor signal, which exists over and above the linear contribution from each motor unit alone. Comparison of the significant features in Fig. 16 outside the 95% confidence limits shows that the time-course of this effect is similar to the time-course of the individual linear effects. As discussed in Section VII, the responses in Fig. 16b, c (for u > 0) consist of the interaction between the mechanical reflex response with other oscillatory mechanisms. The main feature in the third order contribution, Fig. 16a, has a similar time-course, which suggests that the correlation acts to enhance the mechanical reflex component of tremor. The section from the third order cumulant has five maxima above the 95% confidence limit, these are located at latencies of +16, +73, +120, +168 and +189 msec. These are very close to the times of the maxima in the second order cumulants listed in Section VII, therefore it seems likely that the third order contribution from the correlation between the two motor unit discharges reflects the same mechanisms as the second order interactions described previously.

The main peak in the third order cumulant occurs at lag v = 4 msec, corresponding to the latency of the peak in the second order cumulant (Fig. 8a). This is further explored in Fig. 17a, which shows the section, $\hat{q}_{x10}(16, v)$, with lag u fixed at 16 msec, which corresponds to a section perpendicular to the one in Fig. 16a and passing through the first

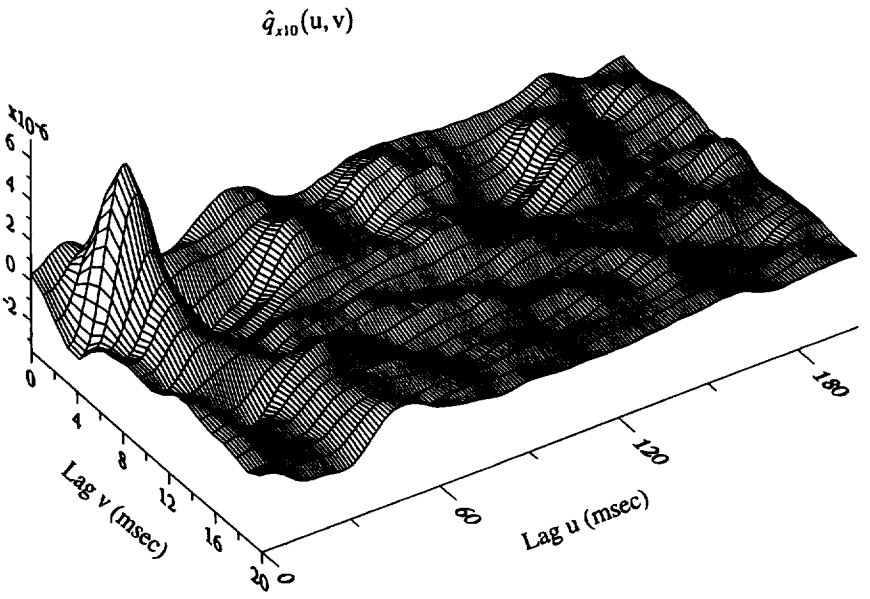

Fig. 15. Surface plot of the estimated third order hybrid cumulant density between motor unit 0, motor unit 1 and tremor, $\hat{q}_{x10}(u, v)$. Plotted for u from 0 to 200 msec, and v from 0 to 20 msec, the origin is at left extremity. The estimate, based on (14.2), is further smoothed with a 2D Hanning type filter before plotting as a surface.

peak at 16 msec. This section shows the range of spacing between motor unit discharges which contributes to the third order cumulant. In Fig. 17b is the second order point process cumulant, $\hat{q}_{10}(u)$ (Fig. 8a), plotted over the same lag range, v = −25 to +25 msec. This illustrates the range of lags over which the two motor units are linearly coupled, and by definition the maximum range over which the third order cumulant can have significant values (since outside these lag ranges the two motor unit discharges are independent, and the third order cumulant will be zero in this area). From Fig. 17 we see that the motor unit discharges contribute to the third order cumulant at all lags over which a second order interaction exists between the discharges.

Turning to the frequency domain, in Fig. 18 is shown an estimate of the magnitude of the third order spectrum, $|\hat{f}_{01x}(\lambda, \mu)|$, (14.9), estimated with T = 1024, and plotted for values of λ, μ up to 50 Hz. This estimate has two main ridges running parallel to the frequency axes and centred around λ, $\mu = 10.7$ Hz. These two frequencies represent a contribution from the motor unit discharges to frequency components around 21.4 Hz in the tremor. This frequency lies within the range defined by the mechanical reflex component (20 Hz) and the higher frequency neurogenic component (28 Hz, see Fig. 3c). Two sections through this estimate are shown in Fig. 19, $|\hat{f}_{01x}(10.7, \mu)|$ (Fig. 19a), and $|\hat{f}_{01x}(\lambda, 10.7)|$ (Fig. 19b), plotted up to 75 Hz. The fixed frequency of each section, determined from the peak, is close to the frequency of the fundamental peak in the estimated auto-spectra in Fig. 3a, b. These sections show the extent of the two ridges running parallel to the axes, and suggest that the third order interaction between the two motor unit discharges can contribute to a broad range of frequencies in the tremor.

Figure 20 shows an estimate of the coefficient (14.10), $\hat{B}_{01x}(\lambda, \mu)$, constructed with T = 512 (L = 351), and plotted for values of λ, μ up to 50 Hz. Two distinct features are apparent in this surface plot, one at low frequencies, around 2 Hz, and a second around 25 Hz. The significance of these peaks is explored in Fig. 21 which shows two sections at fixed frequencies of $\lambda = 2$ Hz, and $\lambda = 21.5$ Hz. Also included is an estimate of the 95% confidence limit based on the hypothesis of a zero-valued cross bi-spectrum, obtained from (15.4). With T = 512 and L = 351 the value is 0.697. The significant features in these two sections provide evidence to suggest the presence of a non-linear interaction between frequency components of the two motor unit discharges which contributes to the tremor.

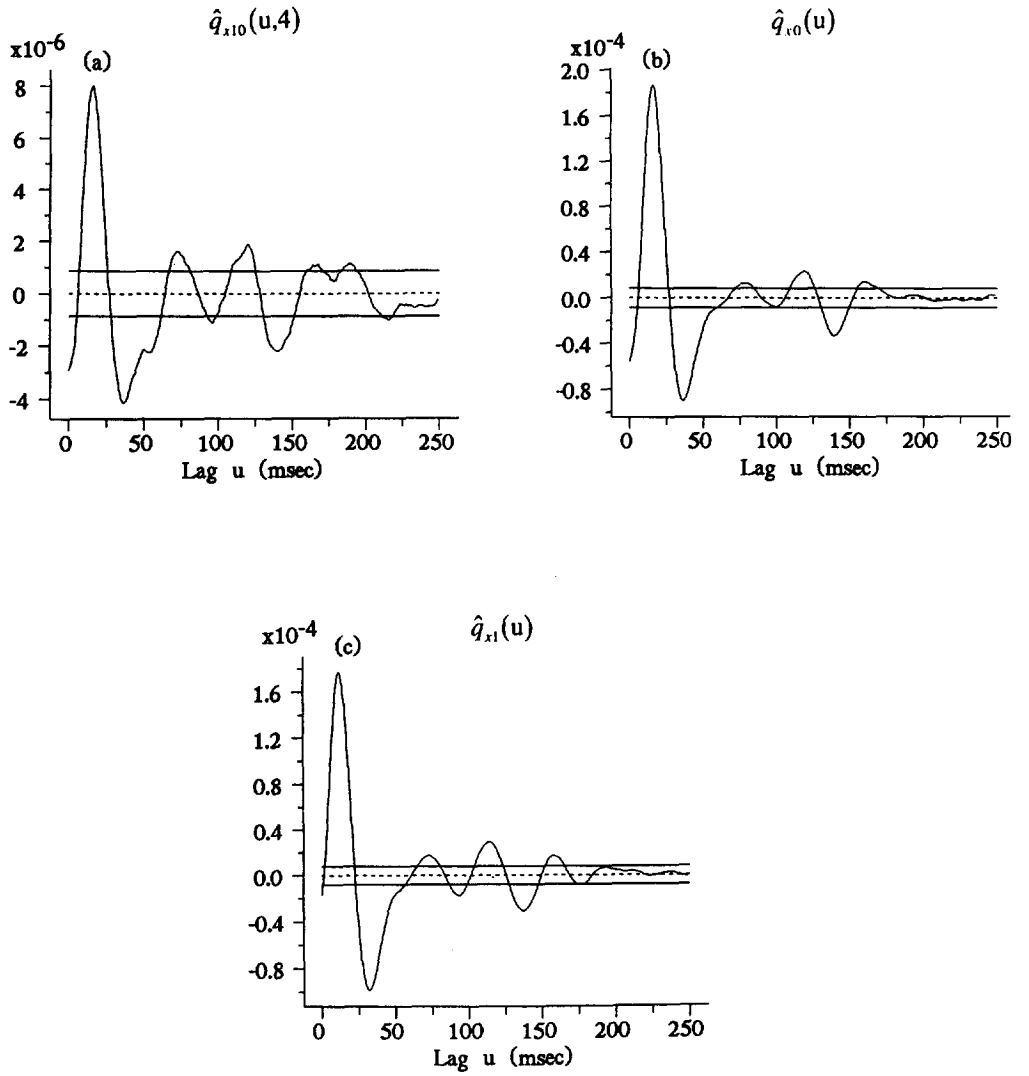

Fig. 16. (a) Section through $\hat{q}_{x10}(u, v)$ at fixed lag $v = 4$, $\hat{q}_{x10}(u, 4)$, and plotted for $u = 0$ to 250 msec. Estimated hybrid cumulant density between (b) motor unit 0 and tremor, $\hat{q}_{x0}(u)$, and (c) motor unit 1 and tremor, $\hat{q}_{x1}(u)$, plotted over the same range of u. The horizontal lines show the asymptotic value (dashed line at zero) and estimated upper and lower 95% confidence limits based on the assumption of independence.

XVII. CONCLUSIONS

In the present report we have set out a comprehensive framework for Fourier-based analysis of hybrid point process/time series data, illustrating the complementary nature of time and frequency domain parameters. This approach also provides a unified framework within which to investigate linear interactions for pure point process data, and pure time series data. Confidence limits for parameter estimates form an important part of the analysis, an aspect often overlooked in this sort of data analysis.

With respect to the illustrated sample analysis and the two questions posed about this particular data set in Section II, the main findings can be summarized as follows. Both motor units of the pair make a similar individual contribution to the tremor. In the frequency domain, there is the suggestion that this involves two distinct frequency bands which overlap with the two frequency bands present in the motor unit coupling (Fig. 4). The first order partial coherence between the motor units using the tremor signal as predictor (Fig. 10c) demonstrates conclusively that common frequency components are involved. Further, the contribution to tremor from the individual

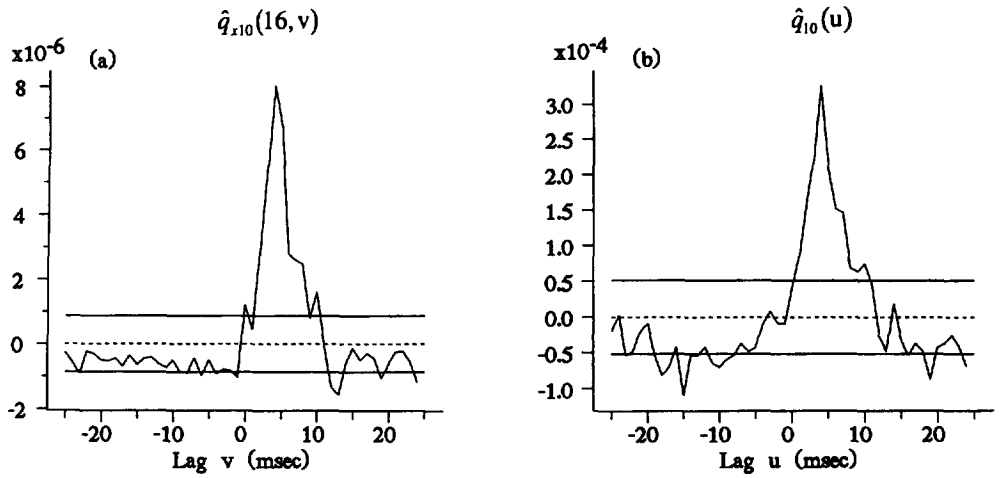

Fig. 17. (a) Section through $\hat{q}_{x10}(u, v)$ at fixed lag $u = 16$, $\hat{q}_{x10}(16, v)$, and plotted for $v = -25$ to $+25$ msec. (b) Estimated point process cumulant density between motor unit 0 and motor unit 1, $\hat{q}_{10}(u)$, plotted over the same range of lags. The horizontal lines show the asymptotic value (dashed line at zero) and estimated upper and lower 95% confidence limits based on the assumption of independence.

minimal at the frequency corresponding to the mean firing rates of the two motor units (Figs. 3, 4). In the time domain the response from individual motor units to tremor has the form of a damped oscillation, with clear organization of the tremor signal before and after motor unit pulses (Fig. 8). Possible interpretations of these features were discussed. A linear systems analysis was seen to give further insight (Figs. 12, 13), and suggested simulation studies to help interpret parameter estimates. There is

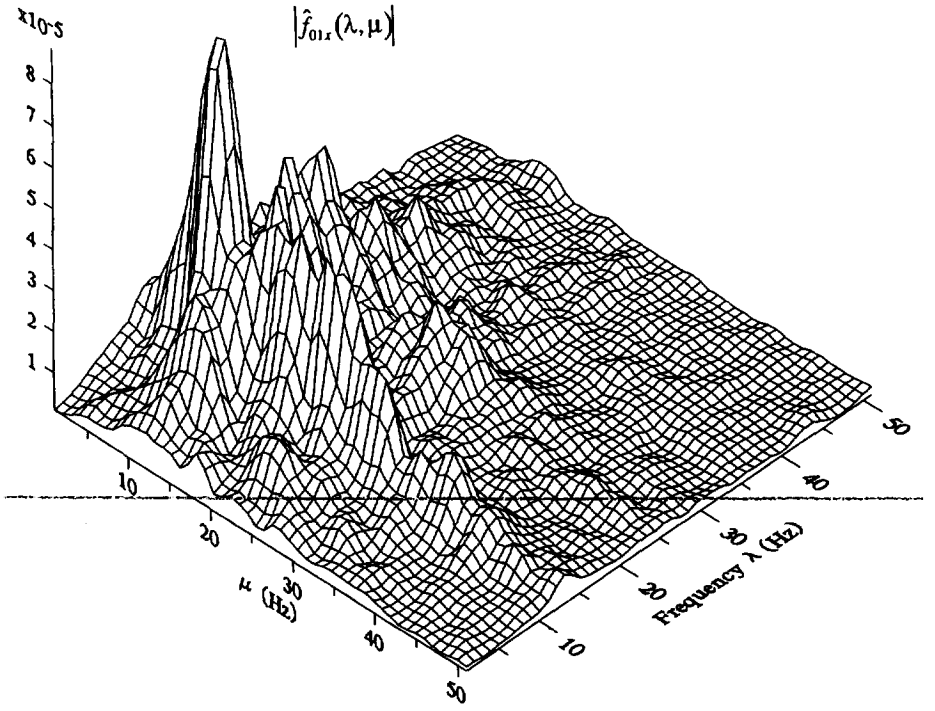

Fig. 18. Surface plot of the magnitude of the estimated third order hybrid spectrum between motor unit 0, motor unit 1 and tremor, $|\hat{f}_{01x}(\lambda, \mu)|$. Plotted for λ, μ up to 50 Hz, origin is at left extremity. The estimate (14.9) is further smoothed with a 2D Hanning type filter before plotting as a surface.

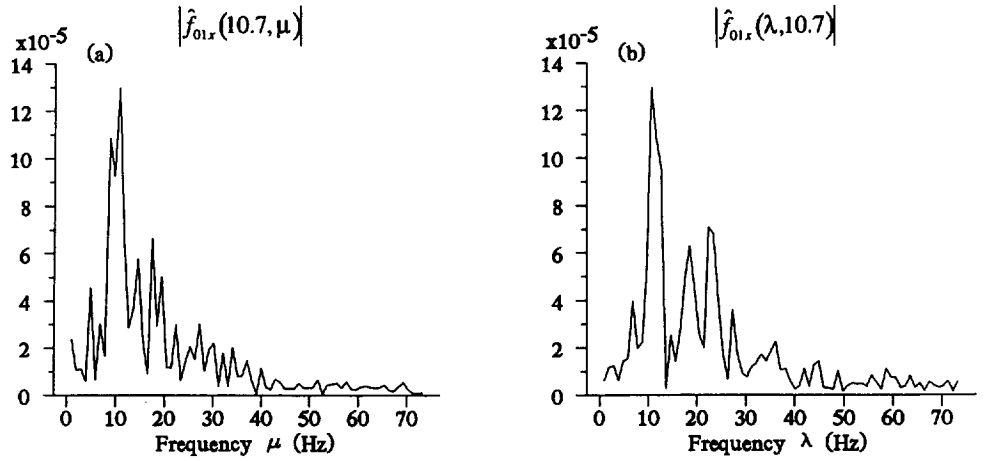

Fig. 19. Sections through the estimated third order hybrid spectrum (a) at fixed frequency $\lambda = 10.7$ Hz, $|\hat{f}_{01x}(10.7, \mu)|$, and (b) at fixed frequency $\mu = 10.7$ Hz, $|\hat{f}_{01x}(\lambda, 10.7)|$.

a significant higher order contribution to the tremor due to the correlated discharge of the motor units (Fig. 15). The estimated third order hybrid cumulant density shows this contribution to have a time-course in response to paired motor unit discharges similar to the contribution from the individual discharges (Fig. 16). A higher order frequency domain analysis suggested the involvement of a range of frequency components in this process (Figs. 18–21). The surface EMG signal proved to be a powerful predictor of motor unit activity with respect to the tremor signal, i.e. parameter estimates showed similar features when the surface EMG was used as a predictor instead of the motor unit discharges (Figs. 4, 6, 8, 12, 13). In the frequency domain the 20–30 Hz region of motor unit coupling was more accurately represented in the surface EMG record than the 0–10 Hz region, this was further illustrated by the

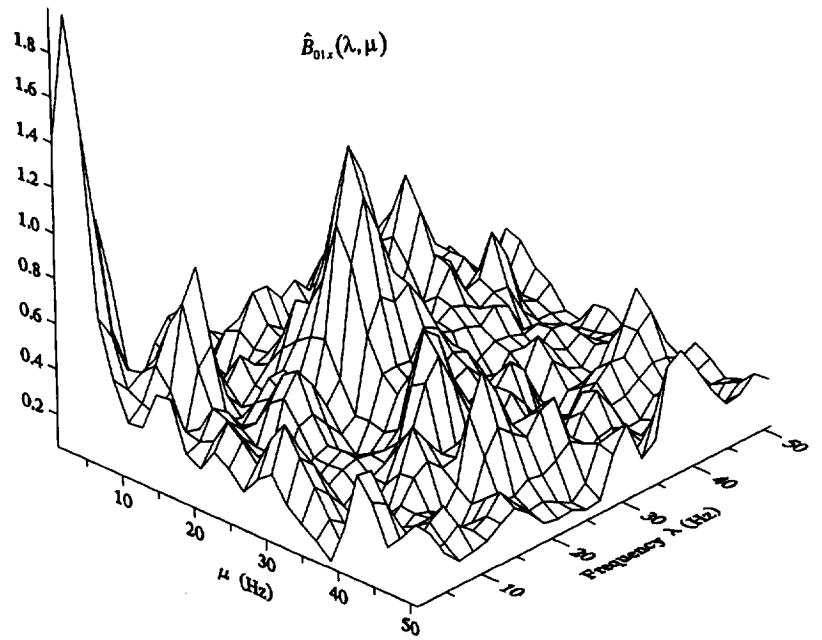

Fig. 20. Surface plot of the magnitude squared of the estimated standardized third order spectral coefficient, $\hat{B}_{01x}(\lambda, \mu)$. Plotted for λ, μ up to 50 Hz, origin is at left extremity. The estimate, based on (14.10), is further smoothed with a 2D Hanning type filter before plotting as a surface.

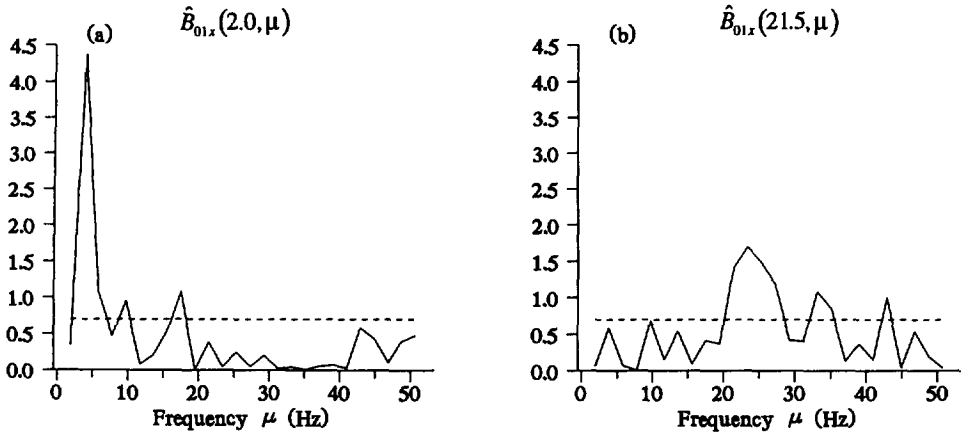

Fig. 21. Sections through an estimate of the coefficient (14.10), $\hat{B}_{01x}(\lambda,\mu)$ (a) at fixed frequency $\lambda=2.0$ Hz, $\hat{B}_{01x}(2.0,\mu)$, and (b) at fixed frequency $\lambda=21.5$ Hz, $\hat{B}_{01x}(21.5,\mu)$. The horizontal dashed lines represents an estimate of the upper 95% confidence limit based on the assumption of a zero valued bi-spectrum.

partial coherence estimate between the two motor units using the surface EMG as predictor (Fig. 10a).

Application of this framework to a single data set has raised some new issues relating to the contribution from motor unit activity to tremor. This demonstrates the utility of the framework. A preliminary analysis of a series of several hundred motor unit/EMG/tremor recordings which incorporate altered inertial loading conditions suggest these findings are robust within and across subjects (Amjad *et al.*, 1994a; Conway *et al.*, 1995).

We conclude with some remarks about the generality of these techniques and suggestions for implementation. An early study using spectral-based regression techniques was that of Groves and Hannan (1968) who studied the effects of sea level on weather. This was based on 3.76 years of hourly observations of eight variables, in total 33,000 samples per variable. They concluded that "Such linear regression studies in the frequency domain may be of marginal worth except in cases where the series lengths are much greater . . ." and ". . . the presentation of these data may have served largely to illustrate the confidence intervals . . . and to emphasize the need of greater degrees of freedom in order to arrive at meaningful conclusions." The message is clear, and equally applicable to the present analysis. Our data set consists of 180,000 observations, any useful inferences which can be made from the parameter estimates may be due in part to the large number of observations available. This is especially true for data with weak correlations, as Fig. 5 demonstrates, indeed, if the present data set had 33,000 samples, with $T=1024$ and $L=32$, an estimated coherence of 0.15 would have a 95% confidence limit of [0.027, 0.33], an interval whose width is twice the value of the parameter. Therefore long data sets are required to reduce the variability to sufficient levels to allow reasonably secure inferences from the data. In this respect the neurophysiologist is perhaps in a fortunate situation, by combining data from repeat runs it may be possible to obtain data of sufficient duration to allow weak correlations to be accurately specified. Initial results (Halliday *et al.*, 1995) indicate that some of the above parameter estimates can be combined in large numbers, thus greatly reducing the statistical variability.

While the methods described in this report are largely non-parametric, and the parameter estimates may not easily be related to the mechanisms underlying the interactions between processes, they nevertheless provide a broad, comprehensive and functional description of these interactions. Moreover, the Fourier-based methods presented above are particularly suited to the study of systems that exhibit rhythmicity. In other areas of scientific data analysis, exploratory analysis based on spectral methods, similar to those presented above, have lead to model-based analyses using likelihood methods (see e.g., Brillinger, 1993).

In the present study the higher order parameters were used to answer a specific question relating to the joint dependency between three of the variables. A prerequisite for any meaningful third order analysis between processes is significant second order interactions between the variables, as was the case for the present data. The third order parameter estimates then provided the first clear demonstration of a contribution to tremor from correlated motor unit discharges. Used in this fashion, higher order analyses are useful in investigating specific questions relating to dependencies between processes. However, the increased variability of higher order parameter estimates and the extra effort in implementing these techniques should be considered before an analysis is attempted.

Perhaps the most promising aspect of the present analysis lies in the application of partial parameters. These have allowed definite statements to be made, for example about frequency components in motor unit coupling being transmitted to physiological tremor. Once second order spectra have been estimated partial parameters can be constructed quickly by algebraic combinations of these spectra. In the first order case this can be done without recourse to matrix arithmetic. Experimental protocols designed to take advantage of partial parameters represent one area where the above techniques may be successfully applied to a wider range of neurophysiological problems.

ACKNOWLEDGEMENTS

Supported by The Wellcome Trust (Grant 036928) and ESRC/MRC/SERC HCI Cognitive Science Initiative. AMA was a visiting fellow from The Education Department, Baluchistan Province, Pakistan, sponsored by the Royal Society.

REFERENCES

Abdulaziz, A., Conway, B. A., Lau, J. W. N. and Rosenberg, J. R. (1992) Partial cumulant density analysis of synchronized neuronal discharges. *Neurosci. Lett.* **S42,** S40.

Amjad, A. M. (1989) Identification of point process systems with application to complex neuronal networks. Ph.D. Thesis, University of Glasgow.

Amjad, A. M., Breeze, P., Conway, B. A., Halliday, D. M. and Rosenberg, J.R. (1989) A framework for the analysis of neuronal networks. In *Progress in Brain Research*, Vol. 80, pp. 243–255 (eds. J. H. Allum and M. Hulliger). Elsevier, Amsterdam.

Amjad, A. M., Conway, B. A., Farmer, S. F., Halliday, D. M. and Rosenberg, J. R. (1994) Third-order hybrid cumulant density analysis of the contribution from correlated motor unit discharges to physiological tremor. *J. Physiol.* **476,** 3P.

Amjad, A. M., Conway, B. A., Farmer, S. F., Halliday, D. M., O'Leary, C. and Rosenberg, J. R. (1994) A load independent 30–40 Hz component of physiological tremor. *J. Physiol.* **476,** 21P.

Bartlett, M. S. (1963) The spectral analysis of point processes. *J. Roy. Statist. Soc.* **25,** 264–281.

Bloomfield, P. (1976) *Fourier Analysis of Time Series: An Introduction.* Wiley, New York.

Brillinger, D. R. (1965) An introduction to polyspectra. *Ann. Math. Statist.* **36,** 1351–1374.

Brillinger, D. R. (1972) The spectral analysis of stationary interval functions. In *Proc. Sixth Berkeley Symposium Math. Statist. Probab.*, pp. 483–513 (eds. L. M. LeCam, I. Neyman and E. Scott). University of California Press, Berkeley.

Brillinger, D. R. (1974) Fourier analysis of stationary processes. *Proc. IEEE* **62,** 1628–1643.

Brillinger, D.R. (1975a) Estimation of product densities. In *Proceedings Computer Science and Statistics 8th Annual Symposium on the interface*, pp. 431–438. Health Science Computing Facility UCLA, Los Angeles.

Brillinger, D. R. (1975b) Identification of point process systems. *Ann. Probab.* **3,** 909–929.

Brillinger, D.R. (1978) Comparative aspects of the study of ordinary time series and of point processes. In *Developments in Statistics*, Vol 1, pp. 33–133, New York. (ed. P. R. Krishnaiah). Academic Press, New York.

Brillinger, D.R. (1981) *Time Series - Data Analysis and Theory*, 2nd edn. Holden Day, San Francisco.

Brillinger, D.R. (1983) The finite Fourier transform of a stationary process. In *Handbook of Statistics*, pp. 21–37 (eds. D. R. Brillinger and P. R. Krishnaiah), Elsevier, Amsterdam.

Brillinger, D. R. (1993) The digital rainbow: some history and applications of numerical spectrum analysis. *Can. J. Statist.* **12,** 1–19.

Brillinger, D. R and Rosenblatt, M. (1967) Computation and interpretation of Kth-order spectra. In *Spectral Analysis of Time Series*, pp. 189–232 (ed. B. Harris). John Wiley, New York.

Brillinger, D .R., Bryant, H .L. and Segundo, J. P. (1976) Identification of synaptic interactions. *Biol. Cybernet.* **22,** 213–228.

Conway, B. A., Halliday, D. M. and Rosenberg, J. R. (1993) Detection of weak synaptic interactions between single Ia-afferents and motor-unit spike trains in the decerebrate cat. *J. Physiol.* **471,** 379–409.

Conway, B. A., Farmer, S. F., Halliday, D. M. and Rosenberg, J. R. (1995) On the relation between motor-unit discharges and physiological tremor. In *Alpha and Gamma Motor Systems*, pp. 596–598 (eds. A. Taylor, M. H. Gladden and R. Durbaba). Plenum, New York.

Elble, R. J. and Koller, W. C. (1990) *Tremor.* Johns Hopkins University Press, Baltimore.

Farmer, S. F., Bremner, F. D., Halliday, D. M., Rosenberg, J. R. and Stephens, J. A. (1993) The frequency content of common synaptic inputs to motoneurones studied during voluntary isometric contraction in man. *J. Physiol.* **470,** 127–155.

Godfrey, M. D. (1965) An exploratory study of the bispectra of economic time series. *Appl. Statist.* **14(1),** 48–69.

Groves, G. W., Hannan, E. J. (1968) Time series regression of sea level on weather. *Rev. Geophys.* **6(2),** 129–174.

Halliday, D. M., Amjad, A. M., Conway, B. A., Farmer, S. F. and Rosenberg, J. R. (1995) A method for comparison of several coherence estimates from independent experiments. *J. Physiol.* **487P,** 76P.

Halliday, D. M., Murray-Smith, D. J. and Rosenberg, J. R. (1992) A frequency-domain identification approach to the study of neuromuscular systems—a combined experimental and modelling study. *Trans. Inst. M.C.* **14,** 79–90.

Huber, P. J., Kleiner, B., Gasser, P. and Dumermuth, G. (1971) Statistical methods for investigating phase relations in stationary stochastic processes. *Proc. IEEE, Trans. Audio and Electroacoustics* **AU-19(1),** 78–86.

Jenkins, G. M. (1963) Contribution to the discussion of a paper by M. S. Bartlett. *J. Roy. Statist. Soc.* **25,** 290–291.

Jenkins, G. M. and Watts, D. G. (1968) *Spectral analysis and its applications.* Holden Day, San Francisco.

Mendel, J. (1991) Tutorial on higher-order statistics (spectra) in signal processing and system theory: theoretical results and some applications. *Proc. IEEE* **79,** 278–305.

Moore, G. P., Segundo, J .P., Perkel, D .H. and Levitan, H. (1970) Statistical signs of synaptic interaction in neurones. *Biophys. J.* **10,** 876–900.

Nikias, C. L. and Raghuveer, M. R. (1987) Bispectrum estimation: a digital signal processing framework. *Proc. IEEE* **75,** 869–891.

Rigas, A. (1983) Point Processes and Time Series Analysis: Theory and Applications to Complex Physiological Systems. Ph.D. Thesis, University of Glasgow.

Robinson, E. A. (1982) A historical perspective of spectrum estimation. *Proc. IEEE* **70,** 885–907.

Rosenberg, J. R., Amjad, A. M., Breeze, P., Brillinger, D. R. and Halliday, D. M. (1989) The Fourier approach to the identification of functional coupling between neuronal spike trains. *Prog. Biophys. molec. Biol.* **53,** 1–31.

Rosenberg, J. R., Murray-Smith, D. J. and Rigas, A. (1982) An introduction to the application of system identification techniques to elements of the neuromuscular system. *Trans. Inst. M.C.* **4,** 187–201.

Rosenblatt, M. (1956) A central limit theorem and a strong mixing condition. *Proc. natn. Acad. Sci.* **42,** 43–47.

Rosenblatt, M. (1983) Cumulants and cumulant spectra. In *Handbook of Statistics,* Vol. 3, pp. 369–382 (eds. D. R. Brillinger and P. R. Krishnaiah). North Holland, New York.

Stiles, R. N. and Randall, J. E. (1967) Mechanical factors in human tremor frequency. *J. appl. Physiol.* **23(3),** 324–330.

Subba Rao, T. and Gabr, M. M. (1984) An introduction to bispectral analysis and bilinear time series models. Springer-Verlag, Berlin.

Wiener, N. (1930) Generalized harmonic analysis. *Acta. Math.* **55,** 117–258.